Next Generation Ground-Motion Prediction Equations for Indo-Gangetic Plains, India

Chhotu Kumar Keshri
Indian Institute of Technology Kharagpur
William Kumar Mohanty (wkmohanty@gg.iitkgp.ac.in)
Indian Institute of Technology Kharagpur

Research Article

Keywords: Ground motion prediction equation, nonlinear regression analysis, peak ground acceleration, pseudo-spectral acceleration, Indo-Gangetic plains, Response spectra.

Posted Date: December 6th, 2021

DOI: https://doi.org/10.21203/rs.3.rs-1137111/v1

Next Generation Ground-Motion Prediction Equations for Indo-Gangetic Plains, India

Chhotu Kumar Keshri[1] and William Kumar Mohanty[1] (*)

[1]Mr. Chhotu Kumar Keshri

keshri.bhu@gmail.com

keshri@iitkgp.ac.in

Department of Geology and Geophysics

Indian Institute of Technology, Kharagpur,

West Bengal-721302, India

[1] Prof. William K. Mohanty. Ph.D.

Professor and Head DS Center of Excellence in Petroleum Engineering
Department of Geology & Geophysics
Indian Institute of Technology, Kharagpur
West Bengal-721302, India.
E-mail: wkmohanty@gg.iitkgp.ac.in
wkmohanty@gmail.com
Phone-91-3222-283360 (Office)
91-3222-283361(Res.)
Fax -91-3222-282268/255303
Mobile: +91-9434083361

(*) Corresponding author

ABSTRACT

India's Indo-Gangetic Plains (IGP) and its proximity to the Himalayas are seismically the most vulnerable zone. For seismic hazard analysis, it requires a reliable Ground Motion Prediction Equations (GMPEs) for this region. The strong motion accelerometer data are used for the present study from 2005 to 2015. PSA of 5% damped linear pseudo-absolute acceleration response spectra at 27 periods ranging from 0.01 s to 10 s used for regression. Two-stage nonlinear regression is used to train the functional form of a nonlinear magnitude scaling, distance scaling, and site conditions. The model includes a regionally independent geometric attenuation finite fault distance metric, style of faulting, shallow site response, basin response, hanging wall effect, hypocentre depth, regionally dependent anelastic attenuation, site conditions, and magnitude-dependent aleatory variability. We consider our new GMPE is valid for earthquakes from active tectonic shallow crustal continental earthquakes for estimating horizontal ground motion for rupture distances ranging from 1 km to 1500 km and magnitudes ranging from 3.3 to 7.9, and focal depth 1-70 km. The proposed GMPEs developed in this study for predicting PGA and PSA are compared with the Campbell and Bozorgnia 2008, 13 and 14, and North Indian GMPEs for IGP, which is agreed upon consistently. Calibration with observed data gives us the confidence to predict the ground motion from the seismic gaps of Himalaya ranges for the Indo-Gangetic plains. The predicted coefficients of the nonlinear model are anticipated to be valuable for probabilistic seismic hazard analysis over the IGP.

Keywords: Ground motion prediction equation, nonlinear regression analysis, peak ground acceleration, pseudo-spectral acceleration, Indo-Gangetic plains, Response spectra.

1. INTRODUCTION

The earthquake mechanism is very complex. As we know, the prediction of occurrences of earthquakes is uncertain. The best possible way to save life and property is by assessing the earthquake hazard and preparing for the risk from future Earthquakes. Ground motion prediction equations (GMPEs) play a crucial role in the hazard assessment in a region. GMPEs are a mathematical expression that relates a strong-motion parameter like peak ground acceleration (PGA) and pseudo-spectral acceleration (PSA) of ground shaking to seismotectonic parameters of the earthquake source, the propagation path between the source and the site, and the surface and subsurface geological layers beneath the site. GMPEs are broadly used to predict the extent of ground shaking at different frequencies. In most regions, a site-specific GMPE is unavailable and ground motions are predicted from GMPEs developed in regions where ground-motion data is available. The purpose of this study is to derive coefficients of a GMPE for the Indo-Gangetic Plains (IGP) in India and reduce variability in ground-motion predictions from currently available models. Insufficiency of strong-motion data has been a core reason for the difficulty in developing GMPEs for IGP India.

There have been endeavours to develop GMPEs for IGP and the northern Himalayas by Raghukanth and Iyengar (NDMA report 2010), Raghukanth et al. (2014), Singh et al. (2017), Srinagesh et al. (2021), Kumar et al. (2019) Anbazhagan et al. (2013), Sharma et al. (2014), Singh et al. (1996), Nath et al. (2005), Harbindu et al. (2014), and Ramkrishnan et al. (2019). The previous models have not considered all the seismotectonic parameters included in other

worldwide models, such as Campbell and Bozorgnia (2014). In the present study, all these seismotectonic parameters have been accounted for. According to Bilham et al. (2001, 2019), about 50 million people in the IGP are at risk from great Himalayan earthquakes. We consider the GMPEs developed in this study to be a reliable model for predicting PGA and PSA from future Himalayan earthquakes. The GMPEs can be used for regional and local-level seismic hazard analysis for sites located on alluvial soil, soft rock, or hard rock conditions in the IGP and adjacent Shiwalik hills. This paper provides a brief description of the database, functional forms, and analyses used to develop GMPEs for IGP, followed by a comparison of the GMPEs model with Campbell and Bozorgnia (2008; hereafter, CB08) and Campbell and Bozorgnia (2014; hereafter, CB14). We also present practical guidance on how to use the model in seismic hazard analysis and engineering applications.

2. INDO-GANGETIC PLAINS SCENARIO

The Himalaya is a convergent plate margin with a high rate of strain accumulation. The nearby IGP consists of four significant sedimentary basins plains, such as the Ganga, Sindhu, Indus, , and Brahmaputra (Fig. 1b). The IGP runs parallel to the seismically active Himalayan mountain chain and is filled with Quaternary sediments. This makes the region highly vulnerable to the severe effects of large earthquakes. The Himalayan region has experienced three large and three two earthquakes in the last century: the 1905 Kangra (**M**~7.8), 1934 Bihar-Nepal (**M**~8.2), 1950 Assam (**M**~8.6), 2005 Kashmir (**M**~7.6), and 2015 Gorkha (**M**~7.8) (Ambraseys and Douglas, 2004; Bilham, 2004, 2008, 2019). Most of the cities located on the IGP come under seismic zone III of the Indian building code,(BIS 2002) where earthquakes are not frequent but the risk is relatively high due to the possible occurrence of large and great Himalayan earthquakes. Far-field amplification effects have been observed

during deep focus (about 200 km deep) earthquakes in the Hindukush mountain ranges due to the soft layered sediments in the IGP and the unusually strong ground motions from these deep-focus earthquakes. The sediments in the IGP are as deep as 8 km (GSI, 2000). There is a good chance of site amplification over a wide range of spectral periods due to the combination of soft shallow sediments and deep sedimentary basins in the IGP from Himalayan region earthquakes and, more specifically, from future earthquakes in the central seismic gap of the Himalaya.

A seismic gap can be defined as a region or fault segment where large or great earthquakes have occurred in the past, but none have happened recently. McCann et al. (1979) defined *seismic gap* as the likelihood of the beginning of great earthquakes along the plate boundaries. The three main seismic gaps in the Himalayan region are the Kashmir, Central, and Assam (Khattri and Wyss, 1978; Khattri, 1987, 1993; Seeber and Armbruster, 1981). The region between the 1934 Bihar-Nepal earthquake and the 1905 Kangra earthquake is known as the Central seismic gap (Fig. 1); the length of this gap is about 750 km. In 1505, a catastrophic earthquake occurred in the Central seismic gap, which caused significant damage over the Ganga basin. Other events that have occurred in the Central seismic gap are the large (**M**~7.0-7.9) 1803 and 1833 earthquakes and the major (**M**~6.0-6.9) 1991 Uttarkashi and 1999 Chamoli .However, because of their relatively small size, these are not the gap-filling earthquakes (Bilham, 1995; Khattri, 1999).

In 2015, a major earthquake occurred in Nepal (**M** 7.9 close to the Central seismic gap. It was not a Central gap-filling earthquake because the rupture propagated east-southeast from the hypocentre away from the seismic gap for about 160 km (Wenyuan et al., 2015). Great earthquakes of magnitude **M** > 8.0 in the Himalayan region are possible in the three identified seismic gaps, and apart from this, the urbanization and population growth over the IGP

126 enhances the risk of physical damage and socio-economic disruption from these earthquakes.
127 Therefore, there is an urgent need to develop new GMPEs for the IGP, which will be helpful
128 in the assessment of seismic hazard and risk in this highly-populated region.
129
130 **3. DATABASE**

131 The Indian Institute of Technology Roorkee (IITR) has a Program for Excellence in Strong
132 Motion Studies (PESMOS), which comprises the Himalayan mountain range from Jammu
133 and Kashmir in the west to Meghalaya in the east PESMOS has installed about 290 strong-
134 motion accelerometer stations on the IGP. Recordings from these stations have been
135 processed by PESMOS and the National Centre for Seismology (NCS) of the Ministry of
136 Earth Sciences, Government of India. The database contains accelerograms recorded over
137 694 stations on IGP, but for the preparation of GMPEs, the earthquake data of $\mathbf{M} \geq 3.0$ and
138 focal depth < 60 km recorded from 2005 to 2015 are used and the remaining were removed
139 from the database. The values of PGA and PSA are the geometric mean of the peaks of the
140 two horizontal componentsThe amplitude of the seismic waves at the recording station
141 depends on the site geology, considering the far-field propagation effect coming from longer
142 distances.

143 The selected strong-motion database consists of 515 recordings from 140 earthquakes of
144 moment magnitude ranging from **M =** 3.0-7.9 with rupture distance ranging from 1-1495 km
145 from India, Nepal, Bhutan, Myanmar, and the Iran-Pakistan border. There are recordings at
146 259 alluvium sites, 59 soft rock sites, and 197 hard rock sites based on the site categorization
147 of Mittal et al. (2012). Fig. 2 shows the earthquake locations and recording stations along the
148 Himalaya and IGP used to develop the GMPEs. Fig. 3(a) shows a plot between PGA and the
149 closest distance to rupture (R_{RUP}). Similarly, a plot between magnitude and closest distance to

150 rupture is shown in Fig. 3(b). A plot of magnitude and focal depth is shown in Fig. 3(c). A
151 plot between magnitude and the time-averaged shear-wave velocity in the top 30 m of the site
152 (V_{S30}) is shown in Fig. 3(d). A plot of basement depth and time-averaged shear-wave
153 velocity in the top 30 m of the site (Fig. 3e). The accelerographs are installed in a room on
154 the ground floor of a one- or two-story building or in the free field inside a small fabricated
155 housing (Kumar et al., 2012). The thickness of sediment deposits above basement rock ($Z_{2.5}$)
156 is taken from (GSI, 2000).
157

158 **4. GROUND MOTION MODEL**

159 We used a referenced Ground GMPE approach using the functional form in CB14. Some
160 modifications are done according to this model as required by the data. A final functional
161 form was chosen based on the availability of the data and the parameters necessary for
162 engineering applications such as probabilistic seismic hazard analysis (PSHA).
163

164 **4.1 Regression analysis approach**

165 **4.1.1 Two-stage Regression Method**

166 Many regression methods have been proposed to develop GMPEs, Two commonly used
167 regression methods are the two-stage method first proposed by Joyner and Boore (1981) and
168 refined by Joyner and Boore (1993) and the random-effects method first proposed by
169 Brillinger and Preisler (1984, 1985) and popularized by Abrahamson and Youngs (1992). The
170 two methods have been shown to give virtually identical results when appropriate weights are
171 used in the second stage (Joyner and Boore, 1993). In this paper, the two-stage nonlinear
172 regression method is employed to obtain the final set of coefficients and standard deviations.
173 The two-stage analysis allowed us to partition the variability into within-event and between-
174 event residuals and standard deviations. In the first stage, nonlinear regression is used to fit

175 the model for the recording-specific terms f_{dis}, f_{atn}, f_{hng}, f_{site}, and f_{sed}. The result is a set of
176 amplitude factors (event terms) and their standard deviations. In the second stage, a
177 regression analysis is conducted on the weighted event terms to fit the earthquake-specific
178 terms f_{mag}, f_{flt}, and f_{hyp}. These terms are defined in following sections of the article.
179

180 **4.1.2 Strong motion intensity measures**

181 Strong-motion parameters represent a specific attribute of an earthquake time history or its
182 frequency-domain equivalent. To describe the active ground motion in engineering
183 seismology, the most common peak time-domain parameters used are PGA and, to some
184 extent, peak ground velocity (PGV) and peak ground displacement (PGD). Peak time-domain
185 parameters represent the maximum absolute amplitude of ground motion from a recorded or
186 synthetic accelerogram, velocity, or displacement time series.

187 For the peak frequency-domain parameters, the most common are the response-spectral
188 parameters PSA and pseudo-spectral velocity (PSV). As seismic design procedures have
189 become more advanced, engineers have begun to consider the natural period of artificial
190 structures into their design using a response spectrum. The component of the strong motion
191 intensity measures (IMs) used in our GMPEs is the geometric mean (GM) of the two as-
192 recorded horizontal components. The IMs used in this study are PGA and PSA for 27
193 oscillator periods (T) ranging from 0.01 sec to 10 sec.
194

195 **4.2 Ground motion model formulation:**

196 The natural logarithm of PGA (g) and PSA (g) (Y) in the first-stage regression is fit by the
197 equation

198 $$\ln(Y) = f_{dis} + f_{hng} + f_{site} + f_{sed} + f_{atn} \qquad (1a)$$

199 The events terms (e) from the first-stage regression are fit in the second stage by the equation

200 $$\ln(\mathrm{Y}) = f_{mag} + f_{flt} + f_{hypo} \quad (1b)$$

201 The initial functional forms of the terms in Equations (1a) and 1b) are those in CB14 as
202 defined below.

203

204 **4.2.1 Magnitude Term**

205 $$f_{mag} = \begin{cases} c_1 + c_2\,\mathbf{M}\,; & \mathbf{M} \le 4.5 \\ c_1 + c_2\mathbf{M} + c_3(\mathbf{M} - 4.5)\,; & 4.5 < \mathbf{M} \le 5.5 \\ c_1 + c_2\mathbf{M} + c_3(\mathbf{M} - 4.5) + c_4(\mathbf{M} - 5.5); & 5.5 < \mathbf{M} \le 6.5 \\ c_1 + c_2\mathbf{M} + c_3(\mathbf{M} - 4.5) + c_4(\mathbf{M} - 5.5) + c_5(\mathbf{M} - 6.5); & \mathbf{M} > 6.5 \end{cases} \quad (2)$$

206 where **M** is moment magnitude.**4.2.2 Geometric Attenuation Term**

207 $$f_{dis} = (c_6 + c_7\mathbf{M}) \ln\left(\sqrt{R_{RUP}^2 + c_8^2}\right) \quad (3)$$

208 where R_{RUP} (km) is closest distance to the co-seismic rupture plane.

209 **4.2.3 Style-of-Faulting Term**

210 $$f_{flt} = f_{flt,F} f_{flt,M} \quad (4)$$

211 $$f_{flt,F} = c_9 F_{RV} + c_{10} F_{NM} \quad (5)$$

212 $$f_{flt,M} = \begin{cases} 0; & \mathbf{M} \le 5.0 \\ \mathbf{M} - 5.0; & 5.0 < \mathbf{M} \le 5.5 \\ 1; & \mathbf{M} > 5.5 \end{cases} \quad (6)$$

213 Where F_{RV} is an indicator variable representing reverse and reverse-oblique faulting given as,

214 $$F_{RV} = \begin{cases} 1, & 30^{\circ} < \boldsymbol{\lambda} \leq 150^{\circ} \\ 0, & otherwise \end{cases} \quad (7)$$

215 F_{NM} is an indicator variable representing normal and normal-oblique faulting given as,

216 $$F_{NM} = \begin{cases} 1, & -150^{\circ} < \boldsymbol{\lambda} \leq -30^{\circ} \\ 0, & otherwise \end{cases} \quad (8)$$

217 and λ (°) is rake angle defined as the average angle of slip on the fault.

218 **4.2.4 Hanging-Wall Term**

219 $$f_{hng} = c_{11} f_{hng,R_{RUP}} f_{hng,M} \quad (9)$$

220 $$f_{hng,R_{RUP}} = \begin{cases} 1; & R_{RUP} = 0 \\ (R_{RUP} - R_{JB})/R_{RUP}; & R_{RUP} > 0 \end{cases} \quad (10)$$

221

222 $$f_{hng,M} = \begin{cases} 0; & \mathbf{M} \leq 5.5 \\ (\mathbf{M} - 5.5)[1 + a_2(\mathbf{M} - 6.5)]; & 5.5 < \mathbf{M} \leq 6.5 \\ 1 + a_2(\mathbf{M} - 6.5); & \mathbf{M} > 6.5 \end{cases} \quad (11)$$

223

224 where a_2 is period-dependent, theoretically constrained model coefficients given in the result
225 table 3 same as (Campbell and Bozorgnia 2013,2014) and $R_{JB}(km)$ is closest distance to the
226 surface projection of the co-seismic rupture plane (Joyner-Boore distance).

227

228 **4.2.5 Shallow Site Response Term**

$$f_{site} = \begin{cases} c_{12} ln\left(\frac{V_{S30}}{k_1}\right) + k_2 \left\{\ln\left[A_{1100} + c\left(\frac{V_{S30}}{k_1}\right)^n\right] - \ln[A_{1100} + c]\right\}; & V_{S30} \le k_1 \\ (c_{12} + k_2 n)\ln\left(\frac{V_{S30}}{k_1}\right); & V_{S30} > k_1 \end{cases}$$

(12)

where V_{S30} (m/sec) is the time-averaged shear-wave velocity in the top 30 m of the site, A_{1100} (g) is the median predicted value of PGA on rock with V_{S30} =1100 m/sec (rock PGA).

4.2.6 Basin Response Term

$$f_{sed} = \begin{cases} c_{13}(Z_{2.5} - 1); & Z_{2.5} \le 1 \\ 0; & 1.0 < Z_{2.5} \le 3 \\ c_{14} k_3 e^{-0.75}\left[1 - exp\left(-0.25(Z_{2.5} - 3)\right)\right]; & Z_{2.5} > 3 \end{cases} \quad (13)$$

where $Z_{2.5}$ (km) is depth to the 2.5 km/sec shear-wave velocity horizon beneath the site (sediment depth), which is taken as the depth to basement in this study.

4.2.7 Hypocentral Depth Term

$$f_{hyp} = f_{hyp,H} f_{hyp,M} \quad (14)$$

$$f_{hyp,H} = \begin{cases} 0; & Z_{HYP} \le 7 \\ (Z_{HYP} - 7); & 7 < Z_{HYP} \le 20 \\ 13; & Z_{HYP} > 20 \end{cases} \quad (15)$$

$$f_{hyp,M} = \begin{cases} c_{15}; & \mathbf{M} \le 5.5 \\ c_{15} + (c_{16} - c_{15})(\mathbf{M} - 5.5); & 5.5 < \mathbf{M} \le 6.5 \\ c_{16}; & \mathbf{M} > 6.5 \end{cases} \quad (16)$$

where Z_{HYP} (km) is the hypocentral depth of the earthquake.

4.2.8 Anelastic Attenuation Term

$$f_{atn} = \begin{cases} c_{17}(R_{RUP} - 80); & R_{RUP} > 80 \\ 0, & R_{RUP} \leq 80 \end{cases} \quad (17)$$

4.3 Treatment of Missing Data

In case of missing predictor variables for recordings in the database, they are either estimated using proxies. Missing values of V_{S30} are taken from the proxies defined in Allen and Wald (2009); Heath et.al (2020); Wald and Allen (2007), and Yong et.al, 2015) derived from surfaciale geological units, geotechnical site categories, ground slope, geomorphology, or elevation. Missing values of Z_{HYP} are taken from focal mechanism solutions from the global moment tensor database (CGMT), PESMOS, and NCS. When the finite rupture models were not available, the finite-fault distance variables R_{RUP} and R_{JB} are derived from R_{EPI}, **M**, and back azimuth using the methodology proposed in Thompson and Worden, 2017).

5. ALEATORY VARIABILITY MODEL

Aleatory variability is defined in terms of both the geometric mean (GM) of the two horizontal components and the arbitrary horizontal component of motion.

5.1 Geometric Mean Horizontal Component

Consistent with the two-stage regression analysis used to derive the median value of *Y*, the aleatory variability model for the GM horizontal component is defined by the equation

$$y_{ij} = Y_{ij} + \eta_i + \varepsilon_{ij} \quad (18)$$

where η_i is the between-event (inter-event) residual for event i and y_{ij}, Y_{ij}, and ε_{ij} are the observed value, predicted value, and within-event (intra-event) residual for recording j of

event i, respectively. The independent normally distributed variables η_i and ε_{ij} have zero means and estimated between-event and within-event standard deviations on reference rock or on soil represented by linear site response, τ and ϕ, given by the magnitude dependent equations

$$\tau = \begin{cases} \tau_1; & \mathbf{M} \leq 4.5 \\ \tau_2 + (\tau_1 - \tau_2)(5.5 - \mathbf{M}); & 4.5 < \mathbf{M} < 5.5 \\ \tau_2; & \mathbf{M} \geq 5.5 \end{cases} \quad (19)$$

$$\phi = \begin{cases} \phi_1; & \mathbf{M} \leq 4.5 \\ \phi_2 + (\phi_1 - \phi_2)(5.5 - \mathbf{M}); & 4.5 < \mathbf{M} < 5.5 \\ \phi_2; & \mathbf{M} \geq 5.5 \end{cases} \quad (20)$$

where τ_i and ϕ_i are empirically derived standard deviations.

The total aleatory standard deviation is given by combining the between-event andwithin-event standard deviations by square-root of sum of squares (SRSS) by the equation

$$\sigma = \sqrt{\tau^2 + \phi^2} \quad (21)$$

5.2 Arbitrary Horizontal Component

The aleatory variance of the arbitrary horizontal components (Boore et al., 1997; Boore, 2005; Campbell and Bozorgnia, 2014) can be calculated from the equation

$$\phi_c^2 = \frac{1}{4N}\sum_{j=1}^{N}\left(\ln(y_{1j}) - \ln(y_{2j})\right)^2 \quad (22)$$

Where the subscripts 1 and 2 refer to the two orthogonal horizontal components, *j* is an index representing the recording, and *N* is the total number of recordings. This equation is used to

calculate the values of ϕ_c associated with the database that is used to develop the model. The total standard deviation corresponding to this component is given by the equation.

$$\sigma_{Arb} = \sqrt{\sigma^2 + \phi_c^2} \quad (23)$$

where σ is the total GM standard deviation given by Equation 21.

6. RESULTS AND DISCUSSION

The coefficients determined in the regression are c_1 to c_{17}. In the shallow site response term, the period-independent theoretically constrained coefficients c = 1.88 and n = 1.18 and the theoretically constrained period-dependent coefficients k_1 and k_2 are from CB14. The theoretically constrained period-dependent coefficient k_3 in the basin response term is also from CB14, although technically it is not needed since it is modified by the regression coefficient c_{14}. It is included to be consistent with CB14. The coefficients of the two-stage regression analysis are summarized in from C_1-C_7 in table 1, from C_8-C_{14} in table 2 and from C_{15}-C_{17} and period dependent parameters k_1, k_2, k_3 and a_2 in table 3. The aleatory standard deviations are summarized in table 4.

6.1 EVALUATION OF RESIDUALS

To validate the derived GMPEs, we plot the between-event residuals (η_i) and the within-event residuals (ε_{ij}) for PGA and PSA at spectral periods of 0.05, 0.2, 1, 3, and 5 sec are against selected predictor variables in Fig. 4 to 11. In these plots, a positive residual indicates underestimation by the model and a negative residual indicates overestimation by the model.

Fig. 4 and 5 show between-event residuals as a function of magnitude and hypocentral depth. Fig. 6 to 11 show within-event residuals as a function of magnitude, rupture distance, site velocity, rock PGA, and sediment depth. The plots show no significant trends or biases in the residuals that would indicate that the model is inconsistent with the data.

6.2 MODEL EVALUATION

Fig. 12 to 19 show how the predicted ground motion scales with magnitude, rupture distance, spectral period, and site effects. The values of the predictor variables used to compute the predicted ground motions are given at the top of each plot. Fig. 12 shows the scaling of PGA with distance (attenuation) for magnitudes of 3.5, 4.5, 5.5, 6.5, and 7.5 for a strike-slip fault. Fig. 13 shows a similar plot for PSA at T = 1.0 sec. The scaling of PGA with distance for strike-slip faults compared from our GMPE with CB08 and CB14 is shown in Fig. 14. For the smaller magnitudes and smaller distances, the predicted PGA values from our model are lower and, for larger distances, the PGA values match well with the CB08 and CB14. For a magnitude of 6.5, our GMPE matches well, but and for larger magnitudes at smaller distances, our predicted values are higher than CB08 and CB14 for reverse faults (Fig. 15a and 15b). In the present study, the closest epicentral distance is 15 km, so the scaling at short distances is not well constrained.

Scaling of PGA and PSA at T=1.0 sec with magnitude for strike-slip faults for different rupture distances (5, 15, 25, 50, 100, 300, and 500 km) for our GMPE (Fig. 16 and 17) show that there is a decreasing trend in PGA/PSA with longer distances and increasing trend with higher magnitudes. Fig. 18 shows the scaling of PSA with magnitude for the GMPE, at rupture distances of 10, 20, 50, 80, 150, and 300 km. There is a clear shift in the peak of the spectra from spectral periods of about 0.1 sec to 1 sec at short distances as magnitude increases from around 3.5 to 5.5, where the peak becomes relatively constant. There is also a noticeable shift at larger distances where the spectral peak shifts to longer periods at small magnitudes and broaden considerably at large magnitudes. Scaling of PSA with different site conditions [NEHRP site categories B (V_{S30} = 1070 m/sec), C (V_{S30} = 525 m/sec), D (V_{S30} = 255 m/sec), and E (V_{S30} = 180 m/sec)] and the PGA values at bedrock for the IGP basin (Fig.

19) shows the variation of PSA with respect to the median estimate of bedrock PGA (A_{1100}) from 0.1*g* to 0.7*g*. Fig. 19 clearly shows the nonlinear soil effects and the associated reduction in spectral amplitude for the softer site conditions (NEHRP D and E) as rock PGA increases.

The between-event, within-event, and total aleatory standard deviations for M≤4.5 and M≥5.5 for IGP GMPEs are shown in Fig. 20. Within-event standard deviations (SD) are higher than between events SD for M≥5.5 and vice-versa for M≤4.5. There is a relatively constant increase in between-event and within event standard deviations from 0.01 sec to 0.4 sec, decreasing for higher periods. For both magnitude ranges, the significant increase in standard deviations due to a smaller number of digital recordings and some outliers present in residual for between event and within event impact the value for standard deviation. Comparing the developed equations for recorded site conditions V_{S30}=900 m/sec hard rock site class A using the 1999 Chamoli earthquake, 6.6 M matched well enough for less than 1.0 sec and started deviating for higher periods (Fig. 21). Comparison of the developed equations for recorded site class C conditions V_{S30}=360 m/sec alluvium using the 1999 Chamoli earthquake 6.6 M matched well and started deviating after 0.7 sec (Fig. 22). Spectra were compared with the GMPE for the present study and Pezeshk 2011 and Iynger 2010 for the magnitude 6.5**M** of a reverse fault at rupture distance 40 km and focal depth 10km. (Fig. 23). Comparison of the present GMPEs with published past GMPEs for IGP and Northwest Himalayas are shown in (Fig. 24).

7. USER GUIDANCE

In this section, guidelines are provided for potential users on evaluating the model for seismic hazard analysis.

355

356 **7.1 Limits for applicability**

357 IGP ground motion model is considered to be valid for shallow focus continental earthquakes
358 (0-60 km), occurring in active tectonic regimes for which the limitations for application:

359 • Minimum magnitudes of **M** ≥ 3.3

360 • Maximum magnitude limits of **M** ≤ 7.0 for strike-slip faults, **M** ≤ 7.9 for reverse faults, and
361 **M**≤ 7.8 for normal faults (further Caution for using this GMPEs for **M** > 8.5).

362 • Distances of R_{RUP} = 1-1500 km;

363 • Shear-wave velocities of V_{S30} = 150 −1620 m/sec as the data used are recorded in this range
364 but for regression V_{S30} velocity were used from USGS V_{S30} model.

365 • Sediment depths of $Z_{2.5}$ = 0-12 km

366 • Hypocentral depths of Z_{HYP} = 1-70 km

367 The IGP model is uniformly valid over the entire range of predictor variables listed above.
368 When the model is extrapolated beyond the data limits of the predictor variable, the errors
369 can become large and should be used with caution under such conditions. The applicable
370 range of some predictor variables has not been extended beyond the limits of the data.
371 Additional details and explanations are given in the following sections.

372

373 **7.2 Magnitude**

374 Magnitude scales define the size of an earthquake and it is of many different types, the most
375 common magnitude used in attenuation relations is moment magnitude (**M**), body-wave
376 magnitude ($\mathbf{M_b}$), surface-wave magnitude ($\mathbf{M_s}$) and local magnitude ($\mathbf{M_L}$). There is a
377 propensity to adopt ***M*** as standard for measuring magnitude because it is derived from

seismological properties like seismic moment, which measures the earthquake energy radiation (Hanks and Kanamori, 1979). In this study **M** was used for the Derivation of the IGP model, the upper magnitude limit for strike-slip is 0.2 units smaller than the limit given, and the upper limits for reverse and normal faults are the same as that used in the database. The lower limit for the IGP model to be reliable for earthquakes of magnitude **M** ≥ 3.3 or 0.3 magnitude units above the minor magnitude used in the analysis (Campbell and Bozorgnia 2014).

7.3 Geometric attenuation and anelastic attenuation

The amplitudes of ground motion decrease as the seismic wave propagate away from earthquake source to site. The "Source-to-site distance" is used to know the decrease in ground motion amplitudes. One of the bases of the assumption of the earthquake as point sources or as finite rupture sources is grouped into two categories: epicentral distance (R_{EPI}) and hypocentral distance (R_{HYPO}), which are the distances measured from point source assumption to the site. Hypocentral distance is measured from the point within the Earth where the earthquake rupture initiated to the site. Epicenter distance is the distance between the Earth's surface points from the hypocentre just above the rupture surface to the site. Finite source distances are generally used in attenuation relations first defined by Joyner and Boore (1981), the horizontal distance to the vertical projection of the rupture plane from the site (R_{JB}), second the distance between the seismogenic parts of the rupture plane to the site (R_{SEIS}). In this study, the Rupture distance (R_{RUP}) is used as a finite fault source approximation of the closest horizontal distance to the vertical projection of the rupture plane to the site, and RJB is used to constrain the hanging wall term. Geometric attenuation is constrained for 0-80 km for up to the magnitude **M** 6.8 because higher magnitude data are

recorded beyond 80 km in the database, and their applicability for lower limits might be beyond 15 km. The attenuation rate is anelastic for large distances constrained by higher magnitude earthquakes in the database, for the IGP model used recordings out to R_{RUP} 1495 km. To constrain the anelastic attenuation term, we consider the GMPEs to be most valid at R_{RUP} <=1000 km, beyond which the number of recordings decreases rapidly.

For IGP, R_{RUP} in the1000 km buffer range from site to earthquakes sources should be considered for PSHA studies. Because for source zone characterization for IGP, it needs to consider the far-field effect due to deeper sediments deposits at the proximity of the Himalayas. Many large magnitude earthquakes impact the IGP due to far-field effects, and presently, no proper GMPEs model is there to consider these effects. The lack of proper GMPEs for the IGP region limits us to characterize source zones in the range of 300km for PSHA (Keshri et al.2020). When the source zones for higher magnitude at a distance greater than 300km the unrealistic PSHA results from Himalaya's earthquake zones using GMPEs based on simulated strong motion data.

7.4 Style-of-Faulting

The orientation of slip on the fault plane is known as rake and dip of the fault plane, and it is characterized by the type of faulting or focal mechanism. The type of faulting is typically classified into slip (horizontal slip), reverse (dip-slip with the hanging-wall side up), thrust (same as reverse but with shallow dip), and normal (dip-slip with the hanging-wall side down). Campbell (1981) empirically demonstrated that reverse and thrust-faulting earthquakes have relatively higher ground motions than strike-slip or normal-faulting earthquakes. It has been common practice that strike-slip and normal faulting events are in the same category, and Reverse and thrust faulting events are in another category. For the study of faulting type, we have used the GCMT catalog focal mechanism solution for

magnitude **M** ≥5, and for magnitude **M** < 5 focal mechanism solution of local source region data used from seismotectonic atlas of India (GSI;2000) to define indicator variables F_{RV} and F_{NM} which represents Reverse, Thrust, Normal, Strike-slip, and oblique faulting.

7.5 Hanging-Wall

For the study, those sites on the hanging wall exhibit more significant acceleration than those on the footwall. The hanging wall effect increased the influence of the seismic dynamic loading on structures. For the IGP model, we have modified the NGA-West, 14 hanging wall term. Only the effect due to rupture distance and magnitude were used for regression, and the other term is removed because of insufficiency of the faults data. For constraining the hanging wall, some of the terms related to R_X (km), which is the closest distance to the surface projection of the top edge of the coseismic rupture plane measured perpendicular to its average strike, dip related terms were dropped from regression analysis because these data were not present in the database.

7.6 Shallow Site Response

Local site conditions are defined in terms of near-surface geology, shear-wave velocity, and sediment depth; it describes the earthy material lying directly beneath the site. Usually, local site conditions are categorized as soil and rock (soft or hard) types. Various GMPEs use this classification of the soil would be further divided up into shallow soil, soft soil, firm soil, and very firm soil. Moreover, in recent developments, the rock could be further divided into soft rock and hard rock (Campbell and Bozorgnia 2008, 2013 2014); shear wave velocity VS30 is used for site parameters. In this study, we have used the V_{S30} for local site conditions as alluvium soil site class C, 180 m/sec to 375 m/sec for soils (alluvium soil (slope washed)),

soft rock (sandstones/slates/limestones/dolomites), class B, 375 m/sec to 700 m/sec for Soft to firm rocks and hard rock (quartzite, dolomites, schist, granodiorites, and gneiss) class A 700 m/sec to 1620 m/sec for Firm/hard rocks. In our selected IGP database, the V_{S30} data were calculated using the USGS model, which characterizes the recording sites in 180 ≤ Vs. ≤900, we caution our GMPEs for site category for V_{S30} ≤180 because no single data is used for this model. The upper limit for V_{S30} is 900m/sec of site class A, but data may be recorded in the range of 700 m/sec - 1620 m/sec. The shallow site term in the IGP model approximates an empirical estimate of site response for general site classification, and it is recommended. It may be extrapolated with caution, and it is recommended to go for site response analysis.

7.7 Basin Response

There is a high strain accumulation rate in the Himalaya convergent plate margins, and it releases from time to time in the region. The main fault types for the Himalayan region are mainly Reverse/Thrust faults, and it comes in the category of shallow-crustal earthquakes in active tectonic areas. Sources in the Indo-Gangetic regions deformation rates are generally low and localized in intraplate regions. This region will be highly influenced by the far-field effect of the Hindukush earthquakes and the shallow thrust earthquakes in the central Himalayas and subduction zone in the northeast region. In this study, the shallow focus earthquake is considered (Z_{HYPO} <60 km).

For the IGP model, to see how the basins impact the ground motions, the basement rock depth of sediments ($Z_{2.5}$) is used for the basin response. The IGP model may be valid for the basement depth of 10-12 km, shallow basement depth, and small V_{S30}. The estimate of basin amplification is not predicted well enough because of the jelly-like behaviour of sediment and basement resonance occurs. In this case, site response analysis is essential.

7.8 Hypocentral Depth

Based on an analysis of residuals, the 60 km limit of hypocentral depth shows its dependence on between-event residuals (Fig. 5) showed that the between-event residuals were generally unbiased down to this depth. We recommend that our IGP model not be used for hypocentral depths or depths to the top of rupture greater than 70 km. This depth limit constrains the modeled earthquakes to occur in the shallow lithosphere up to 70 km. This model is not applicable for the Hindukush earthquakes, intermediate focal depth earthquakes (70-200 km).

8. CONCLUSIONS

In the absence of proper GMPEs in the IGP region, Earthquake Strong Motion recordings from the seismically active Himalayan belt recorded on 259 alluvium sites, 59 soft rock sites, and 197 hard rock sites of IGP are used to establish new GMPEs for the IGP region. The data set consists of 515 strong-motion seismic recordings from 140 earthquakes of moment magnitude ranging from **M** 3.0-7.9 with Rupture distance (R_{RUP}) ranging from 1 -1495 km. An attempt has been made in the present paper to develop a new reference GMPE (IGP) same as CB13 and CB14. In previous models for northern India GMPEs, minimal model parameters was used. In the present study, period-dependent magnitude saturation, magnitude-dependent style of-faulting effects, scaling with hypocentral depth, fault dip, geometric attenuation, regionally dependent anelastic attenuation, hanging-wall effects, shallow linear and nonlinear site response, shallow sediment response, and magnitude-dependent nonlinear between-event and within-event aleatory variability

have been taken as model parameters to develop GMPE based on two-stage nonlinear regression analysis.

Though strong motion data for Indian region is less to develop GMPEs, the result shows that the explanatory variables explain the variation in PGA/PSA. PGA/PSA values were calibrated with previous GMPEs for northern India and worldwide for the fitted model. It is also calibrated for the PSA at different periods for the past 1999 **M**6.6 Chamoli earthquake for two different sites. For the alluvium and Hard rock sites, the predicted and observed values are highly correlated. Further, the future IGP model can upgrade for recorded and simulated ground motion parameters from different Himalayan regions. GMP21 will help predict ground motion parameters to compute the seismic hazard risk on the IGP and the adjacent Siwalik region

9. DATA AND RESOURCES

Strong motion database from https://seismo.gov.in/. The Global Centroid Moment Tensor (CMT) catalog is from http://www.globalcmt.org/. The Next Generation AttenuationWest2 (NGA-West2) database is available at https://peer .berkeley.edu/thrust-areas/data-sciences/databases Consortium of Organizations for Strong Motion Observation Systems Virtual Data Center (https://strongmotion center.org/vdc/scripts/earthquakes.plx), Population data from Socioeconomic Data and Applications Center (SEDAC).

10. ACKNOWLEDGEMENTS

We want to thank Dr. Kenneth W. Campbell, Consulting LLC, Beaverton, Oregon USA, for his constructive interactions, suggestions regarding model selection and computation during

the development. We greatly benefitted from his insightful comments on the manuscript, and model prediction improved significantly with fewer datasets. We would also like to thank PESMOS IIT Roorkee Department of Earthquake Engineering and National Center for Seismology (NCS) Ministry of Earth Sciences, Government of India, for providing me strong motion database.

11. STATEMENTS AND DECLARATION

Funding: The authors declare that no funds, grants, or other support were received during the preparation of this manuscript.

Conflict of interest: The authors declare that they have no competing interests.

- This manuscript has not been submitted to, nor is under review at, another journal or other publishing venue.
- The authors have no affiliation with any organization with a direct or indirect financial interest in the subject matter discussed in the manuscript

Author Contributions:

Both author contribution to this study are as follows.

- **Chhotu Kumar Keshri:** Conceptualization, Data curation, Computation, Methodology, Analysis, and Writing- Original draft preparation.
- **William Kumar Mohanty**: Conceptualization, Supervision, Reviewing and Editing.

Data Availability: Data are available on the request from the authors.

548

549 **12. REFERENCES**

550 Abrahamson, N. A. and R. R. Youngs (1992). A stable algorithm for regression analyses

551 using therandom effects model, Bull. Seism. Soc. Am., 82, 505-510.

552

553 Campbell, K. W., and Bozorgnia, Y., 2007. Campbell-Bozorgnia NGA Ground Motion Relations
554 for the Geometric Mean Horizontal Component of Peak and Spectral Ground Motion Parameters,
555 PEER Report No. 2007/02, Pacific Earthquake Engineering Research Center, University of
556 California, Berkeley, CA, 238 pp.

557

558 Campbell, K. W., and Bozorgnia, Y., 2008. NGA ground motion model for the geometric mean
559 horizontal component of PGA, PGV, PGD and 5% damped linear-elastic response spectra for
560 periods ranging from 0.01 and 10.0 s, Earthquake Spectra 24, 139–171.

561

562 Campbell, K. W., and Bozorgnia, Y., 2013. NGA-West2 Campbell-Bozorgnia Ground Motion
563 Model for the Horizontal Components of PGA, PGV, and 5%-Damped Elastic PseudoAcceleration
564 Response Spectra for Periods Ranging from 0.01 to 10 s, PEER Report No.
565 2013/06, Pacific Earthquake Engineering Research Center, University of California, Berkeley,
566 CA, 238 pp.

567

568 Campbell, K. W., and Bozorgnia, Y., 2014. NGA-West2 Ground Motion Model for the Average
569 Horizontal Components of PGA, PGV, and 5% Damped Linear Acceleration Response Spectra
570 Earthquake Spectra, Volume 30, No. 3, pages 1087–1115, August 2014;

571

572 Allen, T. I., and Wald, D. J., 2009, on the use of high-resolution topographic data as a proxy for
573 seismic site conditions (Vs30), Bulletin of the Seismological Society of America, 99, no. 2A, 935-
574 943.

Heath, D., Wald, D. J., Worden, C. B., Thompson, E. M., and Scmocyk, G. (2020). A Global HybridVS30 Map with a Topographic-Slope-Based Default and Regional Map Insets", Earthquake Spectra, vol. 36, 3: pp. 1570-1584.

Wald, D. J., and Allen, T. I., 2007, Topographic slope as a proxy for seismic site condition and amplification, Bulletin of the Seismological Society of America, 97, no. 5, 1379-1395.

Yong, A., Thompson, E.M., Wald, D., Knudsen, K.L., Odum, J.K., Stephenson, W.J., and Haefner, S., 2015, Compilation of Vs30 Data for the United States: U.S. Geological Survey Data Series 978, 8 p.

Thompson, E. M., and C. B. Worden (2017). Estimating rupture distances without a rupture, *Bulletin of the Seismological Society of America*. DOI: https://doi.org/10.1785/0120170174.

Ashok Kumar, Himanshu Mittal, Rajiv Sachdeva, Arjun Kumar (2012)."Indian Strong Motion Instrumentation Network and its site characterization". International Journal of Geosciences, 3(6): 1151-1167. 2

Bilham R., 1995. Location and magnitude of the 1833 Nepal earthquake and its relation to the rupture zones of contiguous great Himalayan earthquakes. Current Science, 69, 2, 101-128.

Bilham, R., Gaur, V. K. and Molnar, P. (2001). Himalyan Seismic Hazard. Science, 293, 1442-1444

Campbell, K. W. (1981). Near-source attenuation of peak horizontal acceleration. *Bull. Seismol. Soc. Am.* **71**, 2039–2070.

602 Campbell, K.W., Bozorgnia, Y. (2003) Updated Near-Source Ground-Motion (Attenuation)
603 Relations for theHorizontal and Vertical Components of Peak Ground Acceleration and
604 Acceleration Response Spectra Bulletin of the Seismological Society of America, Vol. 93, No. 1,
605 pp. 314–331.
606
607 Dasgupta, S. and Mukhopadhyay, B. 1803 earthquake in garhwal himalaya – archival materials
608 with commentary, Indian Journal of History of Science, 49.1 (2014) 21-33
609
610 Dasgupta, S. and Mukhopadhyay, B. Historiography and Commentary on the Nepal -
611 India Earthquake of 26 August 1833, Indian Journal of History of Science, 50.3 (2015) 491-513
612
613 David R. Brillinger, Haiganoush K. Preisler; An exploratory analysis of the Joyner-Boore
614 attenuation data. *Bulletin of the Seismological Society of America* 1984;; 74 (4): 1441–1450.
615 doi: https://doi.org/10.1785/BSSA0740041441
616
617 David R. Brillinger, Haiganoush K. Preisler; Further analysis of the Joyner-Boore attenuation
618 data. *Bulletin of the Seismological Society of America* 1985;; 75 (2): 611–614.
619 doi: https://doi.org/10.1785/BSSA0750020611
620
621 Fan, W., and P. M. Shearer (2015); Detailed rupture imaging of the 25 April 2015 Nepal
622 earthquakeusing teleseismicP waves, Geo-phys. Res. Lett., 42, 5744 5752, doi:
623 10.1002/2015GL064587
624
625 Hanks, T. C., and H. Kanamori (1979). A moment magnitude scale, Journal of
626 Geophysical Research, 84, 5, 2348 – 2350.
627
628 Himanshu Mittal, Ashok Kumar, Rebecca Ramhmachhuani (2012) Indian National Strong Motion
629 Instrumentation Network and Site Characterization of Its Stations, International Journal of
630 Geosciences, 2012, 3, 1151-1167.
631

Joyner, W. B., and D. M. Boore (1981). Peak horizontal acceleration and velocity from strong-motion records including records from the 1979 Imperial Valley, California, earthquake. *Bull. Seismol. Soc. Am.* **71**, 2011–2038.

Joyner, W. B., and D. M. Boore (1993).Methods for regression analysis of strong-motion data Bulletin of the Seismological Society of America, Vol. 83, No. 2, pp. 469-487.

Chhotu Kumar Keshri; William Kumar Mohanty and Pratul Ranjan, (2020), Probabilistic seismic hazard assessment for some parts of the Indo-Gangetic plains, India, Natural Hazards: Journal of the International Society for the Prevention and Mitigation of Natural Hazards, **103**, (1), 815-843

Khattri, K. (1993) Seismic gaps and likelihood of occurrence of larger earthquakes in northern India, 10 June 1993, 64 (11-12)

Khattri, K. (1987) Great earthquakes, seismicity gaps and potential for earthquake disaster along the Himalaya plate boundary, Tectonophysics 138 (1): 79-92

Khattri, K. and M. Wyss (1978). Precursory variations of seismicity in Assam area, India, Geology 6, 685-688.

Khattri, K. (1999) Probabilities of occurrence of great earthquakes in the Himalaya, Indian Acad. Sci. (Earth Planet. Sci.), 108, No. 2, June 1999, pp. 87-92.

McCann, W. R., S. P. Nishenko, L. R. Sykes, and J. Krause, Seismic gaps and plate tectonics: Seismic potential for major boundaries, Pure Appl. Geophys., 117, 1082-1147, 1979

Seeber, L. and J. G. Armbruster (1981). Great detachment and earthquakes along the Himalayan arc and long-term forecasting, in Earthquake Prediction, D. W. Simpson and P. G. Richards, Editors, A.G.U., Washington, D.C., Maurice Ewing Series, 4, 259-277.

Seismotectonic atlas of India and its environs (2000) geological survey of India.Srinagesh et al.(2021) ground motion prediction equation for earthquakes along the western himalayan arc, current science, vol. 120, no. 6, 25

Raghukanth STG, Kavitha B (2014) Ground motion relations for active regions in India. Pure appl Geophys171:2241–2275

Singh SK, Mohanty WK, Bansal BK, Roonwal GS (2002) Ground motion in Delhi from future large/great earthquakes in the central seismic gap of the Himalayan arc. Bull Seismol Soc Am 92:555–569

Iyengar RN (2010) Development of probabilistic seismic hazard map of India. Technical report of WCE constituted by NDMA govt. of India, New Delhi.

Singh, S. K. *et al.* , Strong ground motion in the Indo-Gangetic Plains during the 2015 Gorkha, Nepal, earthquake sequence and its prediction during future earthquakes. *Bull. Seismol. Soc. Am*., 2017, **107**, 1293–1306; doi:10.1785/0120160222.

Pezeshk S, Zandieh A, Tavakoli B (2011) Hybrid empirical ground-motion prediction equations for Eastern North America using NGA models and updated seismological parameters. Bull Seismol Soc Am101 (4):1859–1870

N. N. Ambraseys and J. Douglas. (2004), Magnitude calibration of north Indian earthquakes *Geophys. J. Int* 159, 165–206.

BILHAM, R. 2004. Earthquakes in India and the Himalaya: tectonics, geodesy and history. Annals of Geophysics, 47, 839–858

BILHAM, R. 2008. Tom LaTouche and the Great Assam Earthquake of 12 June 1897; letters from the epicenter. Seism. Res. Lett., 79, 426–437.

691

692 BILHAM, R. 2019. Himalayan earthquakes: a review of historical seismicity
693 and early 21st century slip potential; *Geological Society, London, Special Publications* (2019),
694 483(1):423

695

696 Kumar P, Chamoli BP, Kumar A, Gairola A. Attenuation relationship for peak
697 horizontal acceleration of strong ground motion of Uttarakhand region of central
698 Himalayas attenuation relationship for peak horizontal acceleration of strong
699 ground motion of Uttarakhand region of central. J Earthq Eng 2019:1–18. https://
700 doi.org/10.1080/13632469.2019.1634161. 0.

701

702 Anbazhagan P, Kumar A, Sitharam TG. Ground motion prediction equation
703 considering combined dataset of recorded and simulated ground motions. Soil
704 Dynam Earthq Eng 2013;53: 92–108. https://doi.org/10.1016/j.
705 soildyn.2013.06.003.

706

707 Sharma ML, Douglas J, Bungum H, Kotadia J. Ground-motion prediction equations
708 based on data from the himalayan and zagros regions. J Earthq Eng 2009;13:
709 1191–210. https://doi.org/10.1080/13632460902859151.

710

711 Nath SK, Vyas M, Pal I, Sengupta P. A seismic hazard scenario in the Sikkim
712 Himalaya from seismotectonics, spectral amplification, source parameterization,
713 and spectral attenuation laws using strong motion. seismometry 2005;110:1–24.
714 https://doi.org/10.1029/2004JB003199.

715

716 Harbindu A, Gupta S, Sharma ML. Earthquake ground motion predictive equations
717 for Garhwal Himalaya, India. Soil Dynam Earthq Eng 2014; 66:135–48. https://doi.
718 org/10.1016/j.soildyn.2014.06.018

719

720 Ramkrishnan R, Sreevalsa K, Sitharam TG. Development of new ground motion
721 prediction equation for the north and central Himalayas using recorded strong
722 motion data development of new ground motion prediction equation for the north
723 and central Himalayas using recorded strong. J Earthq Eng 2019:1–24. https://doi.
724 org/10.1080/13632469.2019.1605318. 0

725

726 Singh RP, Aman A, Prasad YJJ. Attenuation relations for strong seismic ground
727 motion in the Himalayan region. Pure Appl Geophys 1996; 147:161–80. https://
728 doi.org/10.1007/bf00876442.

729

730 Center for International Earth Science Information Network (CIESIN), Columbia University;
731 United Nations Food and Agriculture Programme (FAO); and Centro Internacional de Agricultura
732 Tropical (CIAT). 2005. Gridded Population of the World: Future Estimates (GPWFE). Palisades,
733 NY: Socioeconomic Data and Applications Center (SEDAC), Columbia University. Available at

734 http://sedac.ciesin.columbia.edu/gpw.(20/10/2021)

735

736

737

738

739

740

Figures

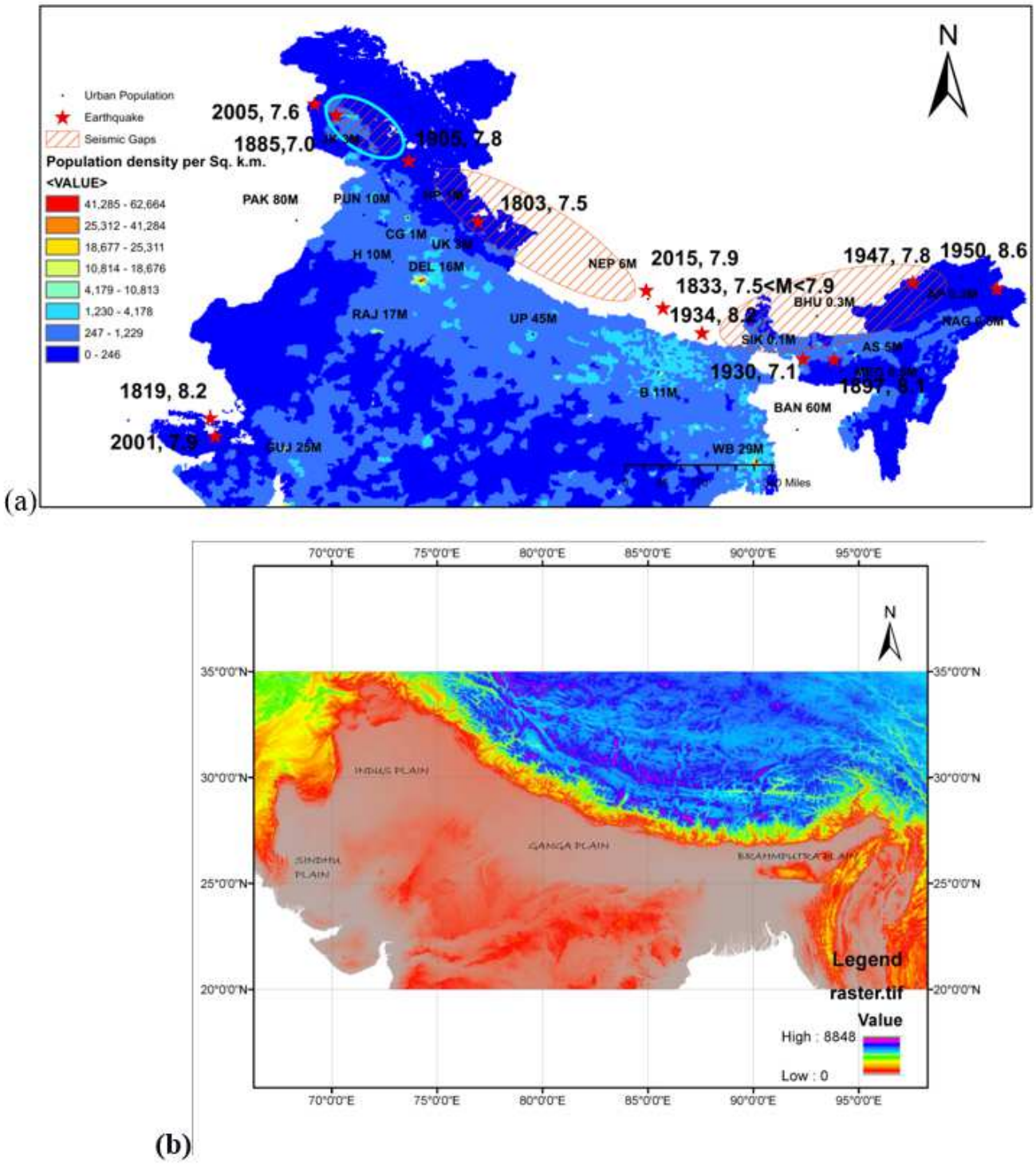

Figure 1

a) Map showing the Increasing urban population and population density on the Indo-Gangetic plains and large-to-great Himalayan earthquakes from the last 200 years. The (from left to right) Kashmir, Central, and Assam seismic gaps, which are expected to generate M > 8 earthquakes, are identified by the hatched zones. b) Ganga, Indus, Sindhu, and Brahmaputra plains.

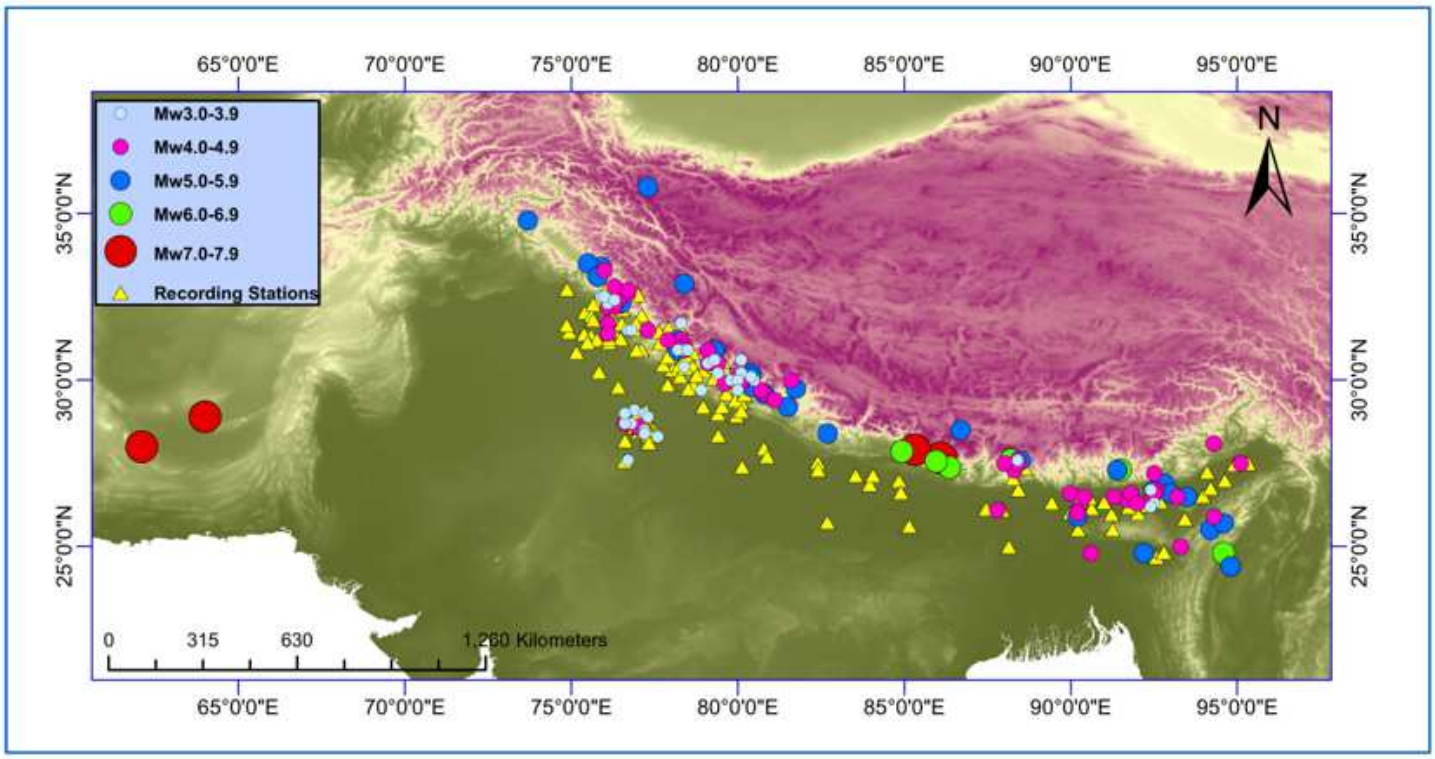

Figure 2

Map showing the distribution of earthquakes of M > 3 and recording stations along the Himalayan mountain range and the IGP used in the development of the GMPEs.

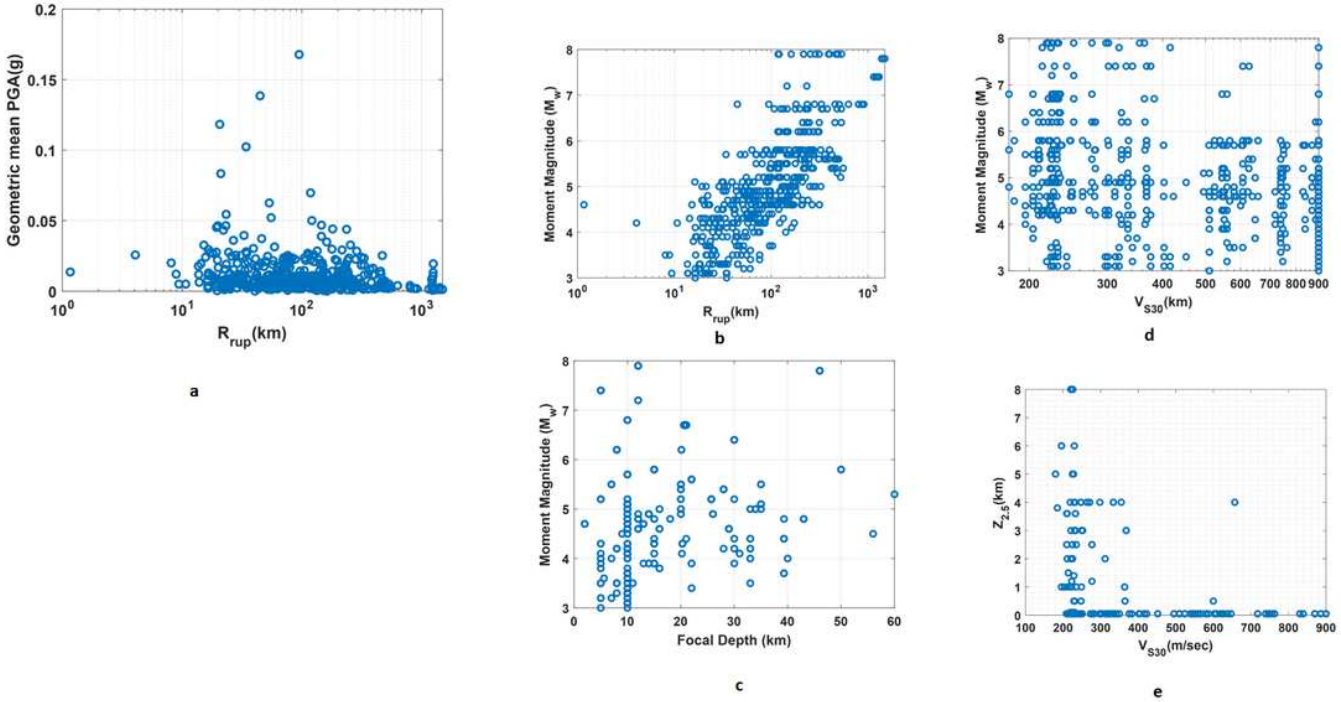

Figure 3

(a) a plot of PGA and closest distance to rupture. (b) a plot of magnitude and closest distance to rupture (c) a plot of magnitude and focal depth. (d) a plot of magnitude and time-averaged shear-wave velocity in the top 30 m of the site. (e) a plot of basement depth and time-averaged shear-wave velocity in the top 30 m of the site.

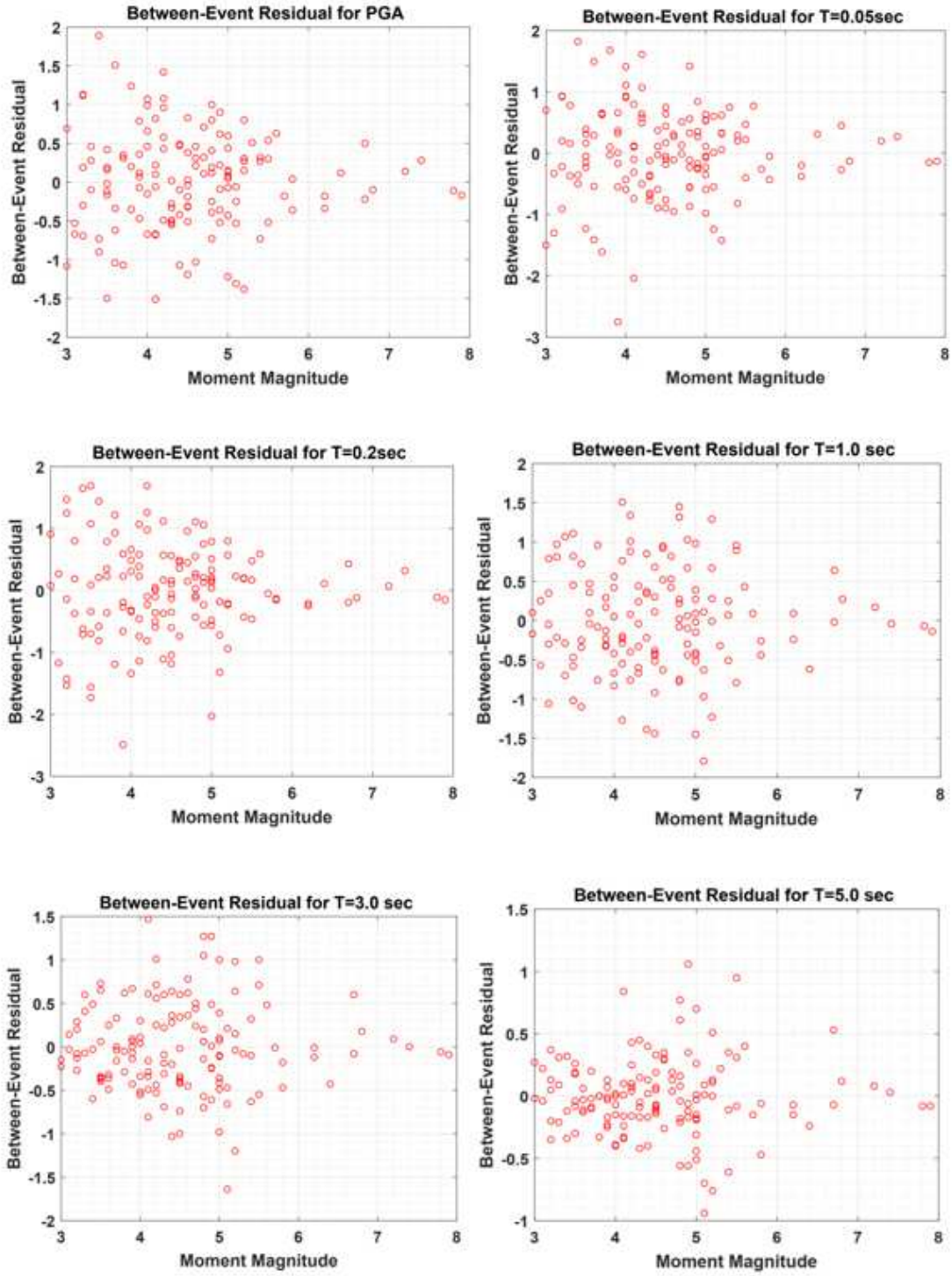

Figure 4

Dependence of between-event residuals on earthquake magnitude.

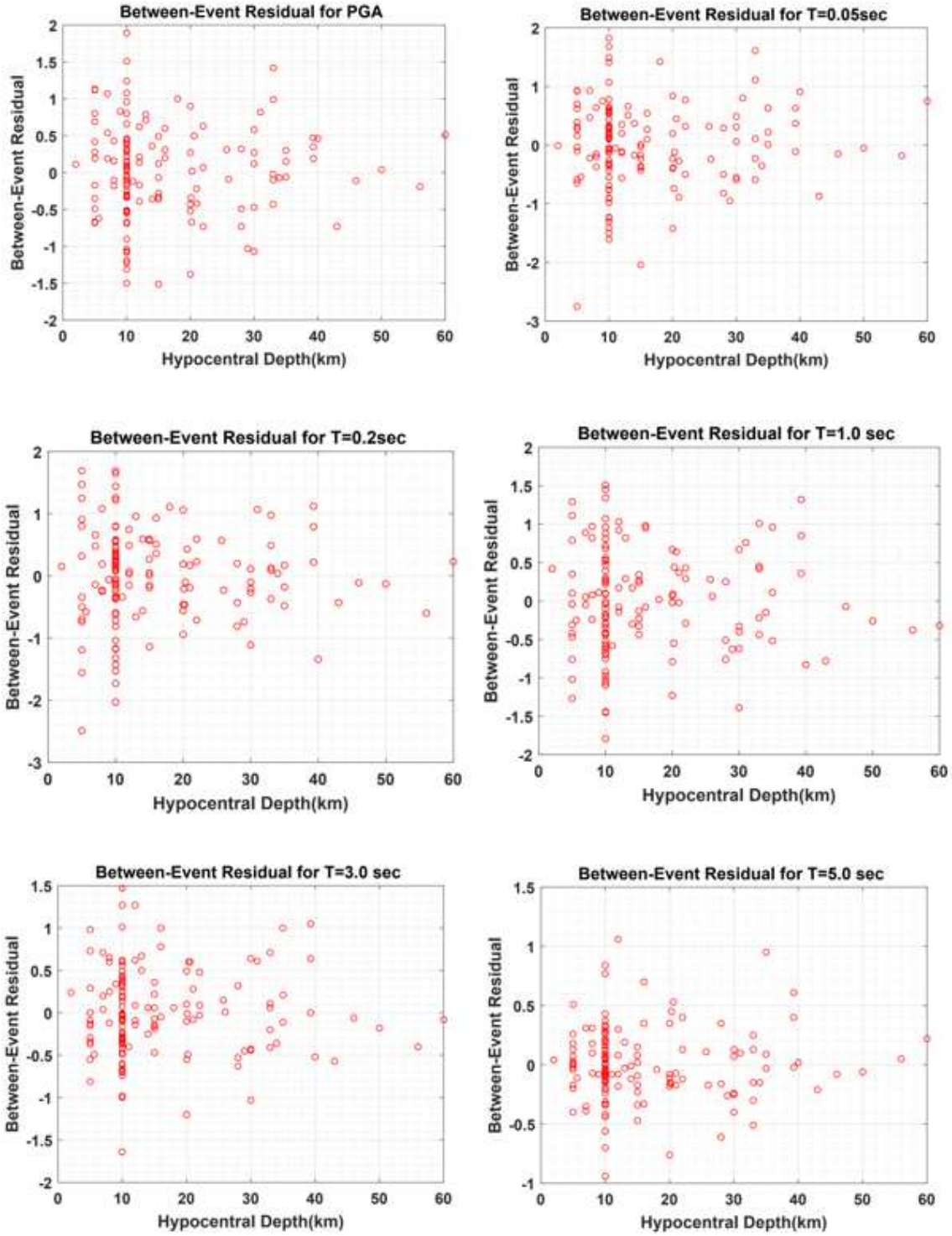

Figure 5

Dependence of between-event residuals on hypocentral depth.

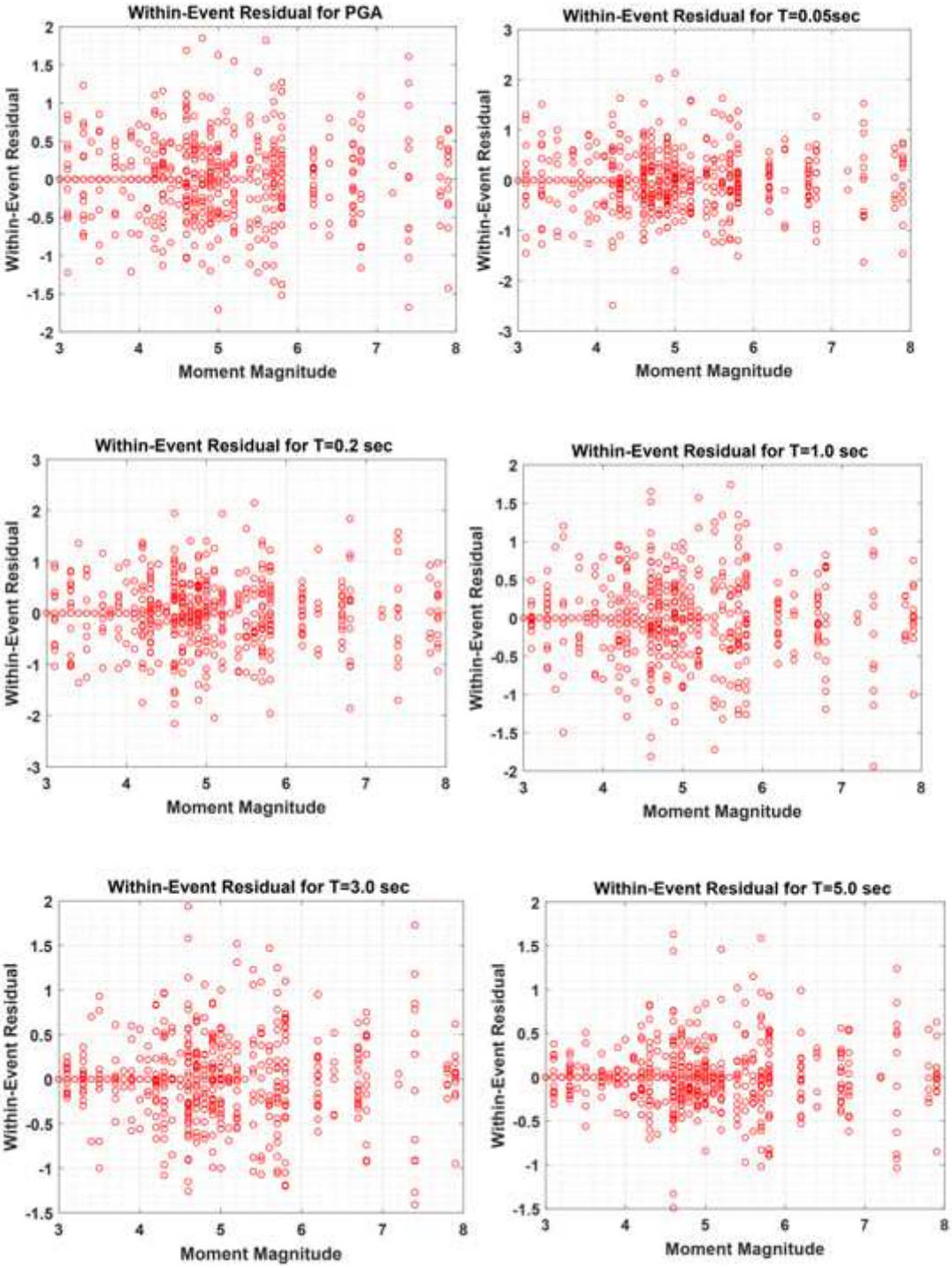

Figure 6

Dependence of within-event residuals on earthquake magnitude.

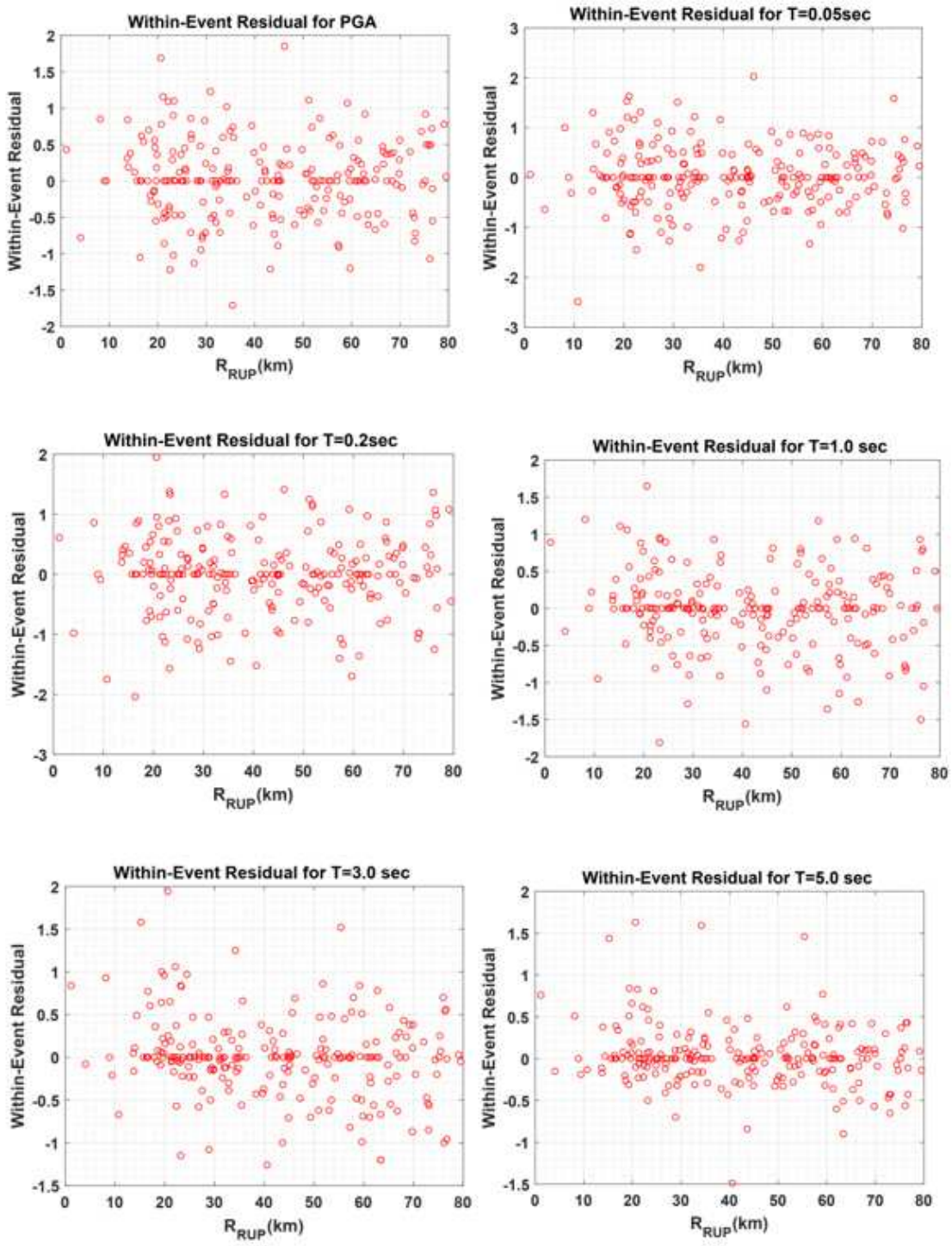

Figure 7

Dependence of within-event residuals on rupture distance for near-source distances ranging from 0 to 80 km.

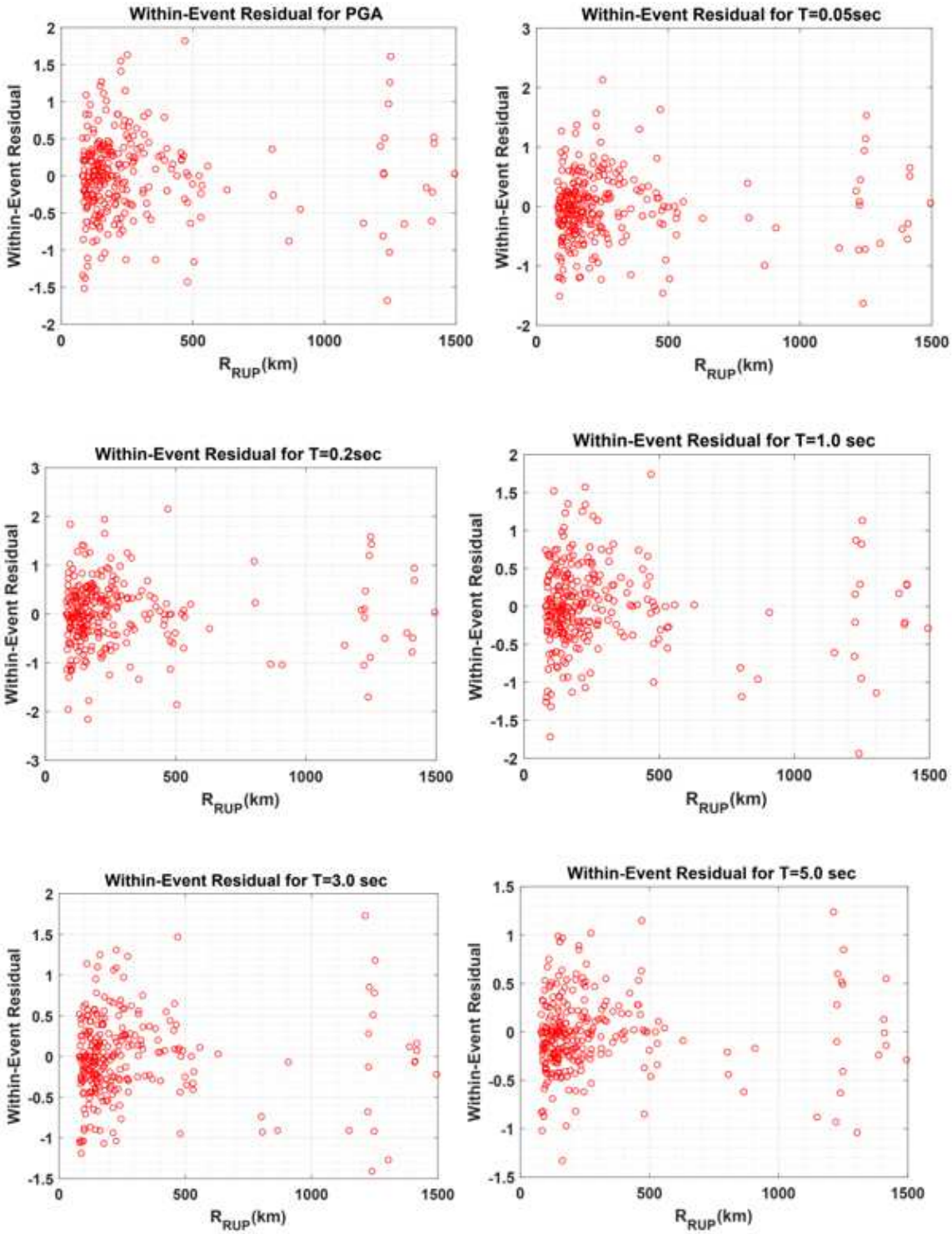

Figure 8

Dependence of within-event residuals on rupture distance for far-source distances ranging from 80 to 1500 km.

Figure 9

Dependence of within-event residuals on site velocity.

Figure 10

Dependence of within-event residuals on sediment (basin) depth.

Figure 11

Dependence of within-event residuals on rock PGA.

Figure 12

Scaling of PGA with distance for the IGP model.

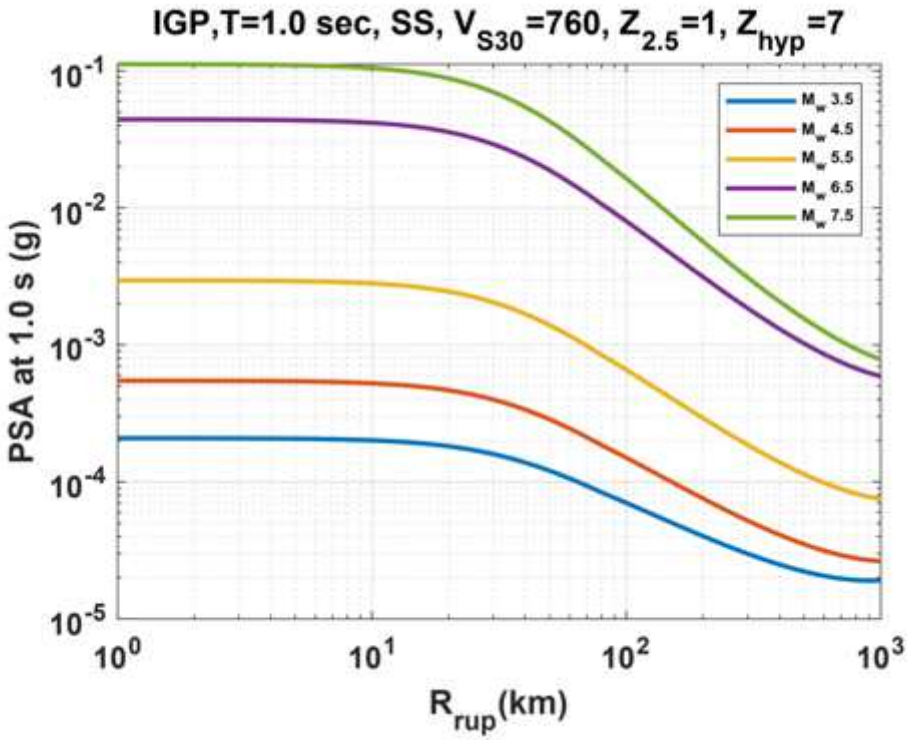

Figure 13

Scaling of PSA at 1.0 sec with rupture distance for the IGP model

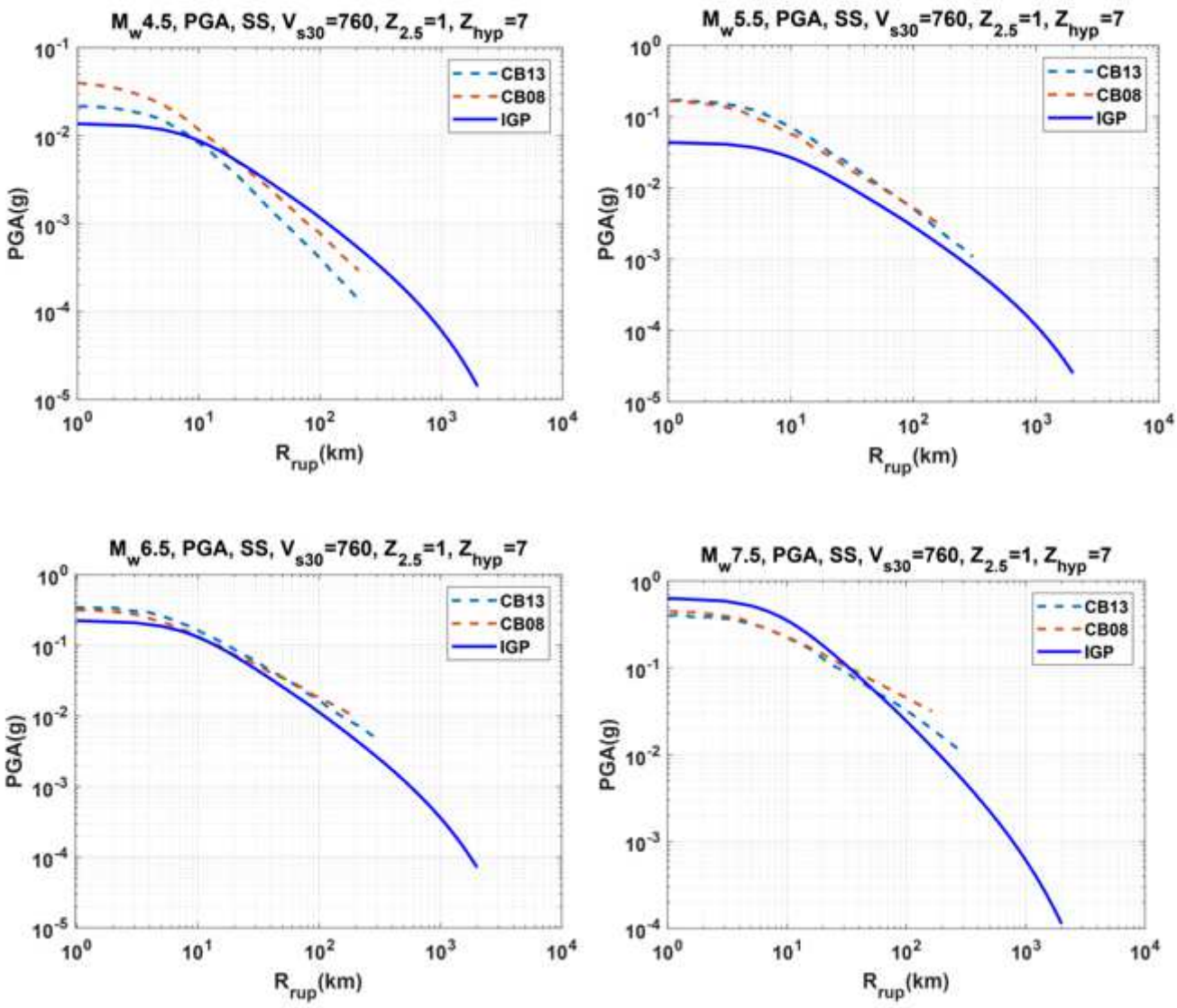

Figure 14

Scaling of PGA with distance for strike-slip faults comparing the IGP, CB08 and CB13, models.

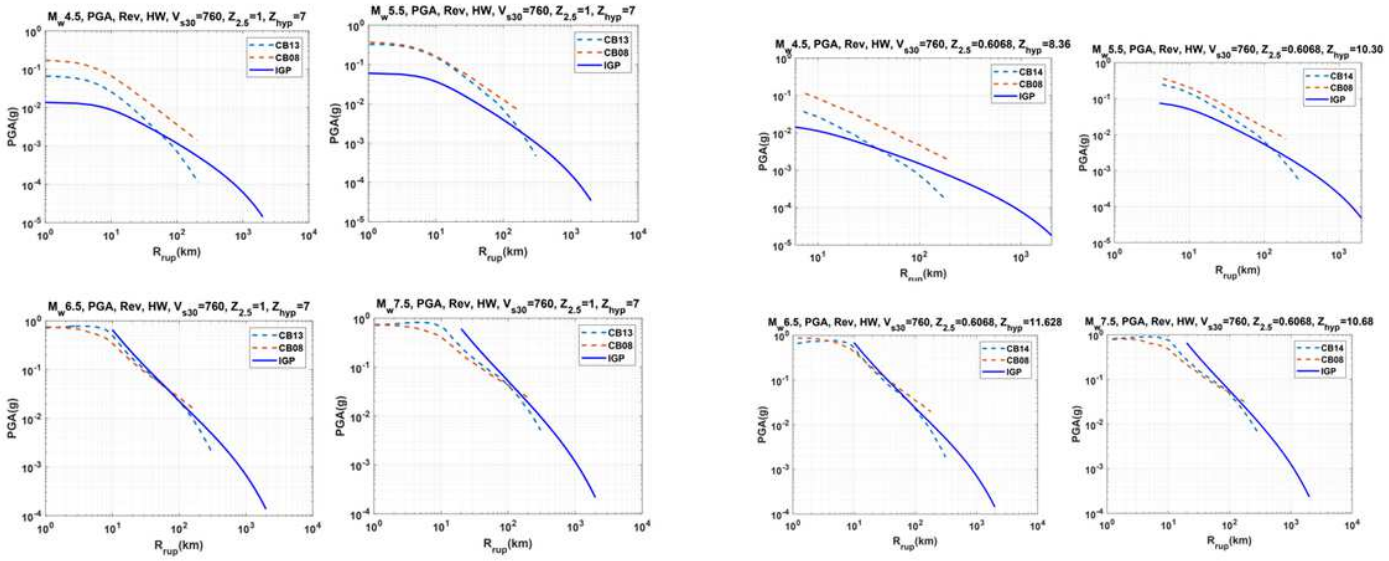

Figure 15

a. Scaling of PGA with distance for reverse faults comparing the CB08 and CB13 models for different magnitudes. b. Scaling of PGA with distance for reverse faults comparing the CB08 and CB14 models different magnitudes, basement depth and hypocentre depths.

Figure 16

Scaling of PGA with magnitude for strike-slip faults for IGP model.

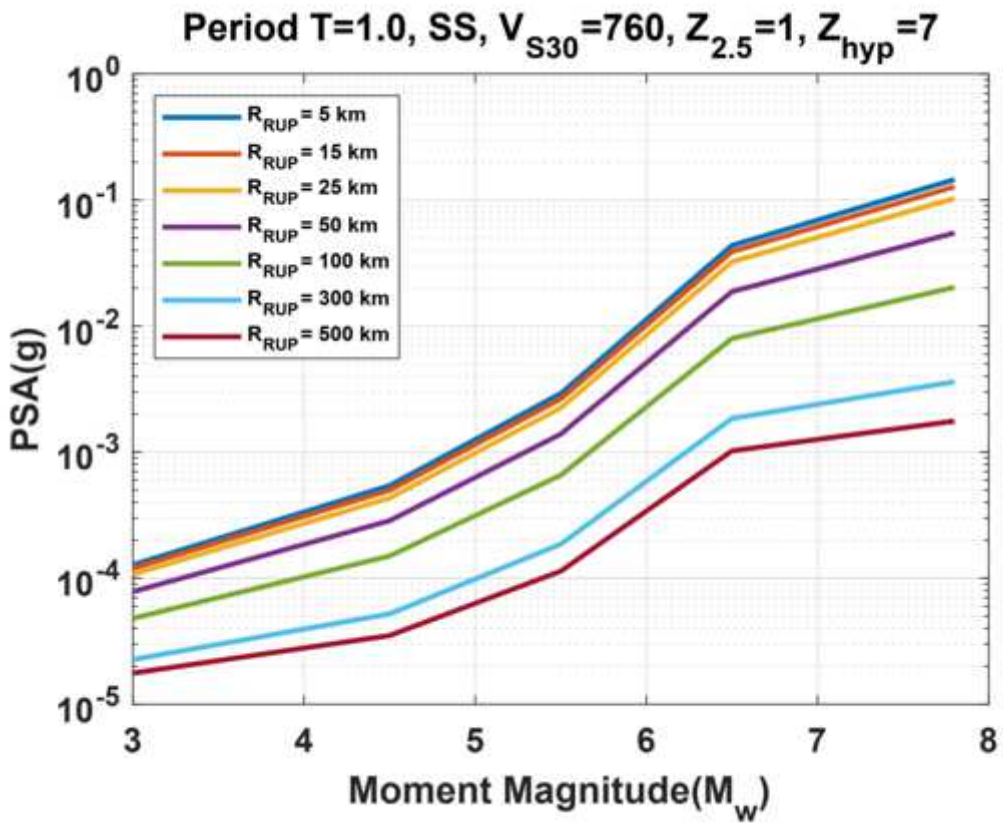

Figure 17

Scaling of PSA with magnitude for strike-slip faults for IGP model.

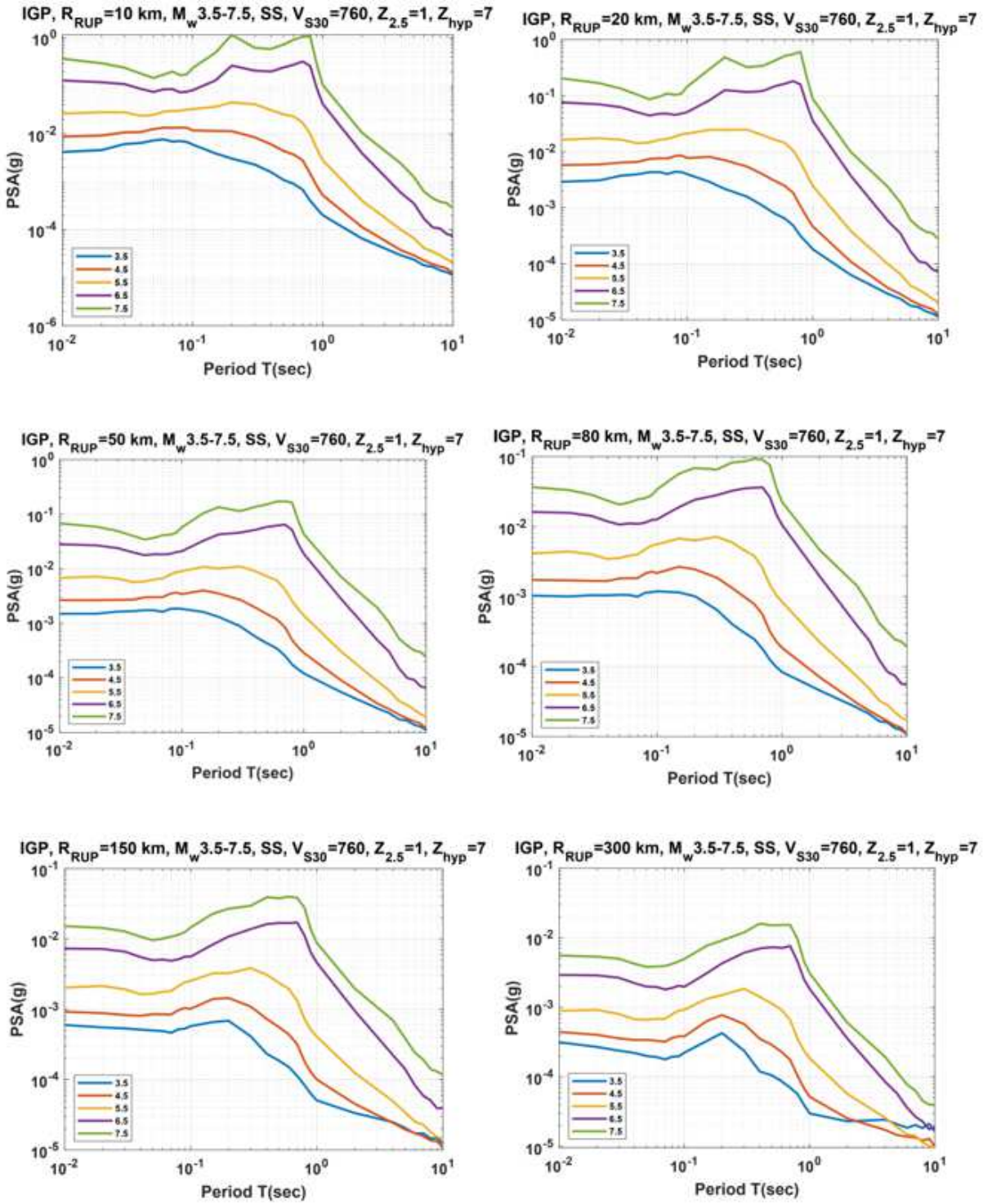

Figure 18

Scaling of PSA with periods (M3.5, 4.5, 5.5, 6.5 and 7.5) for the IGP model for different rupture distances.

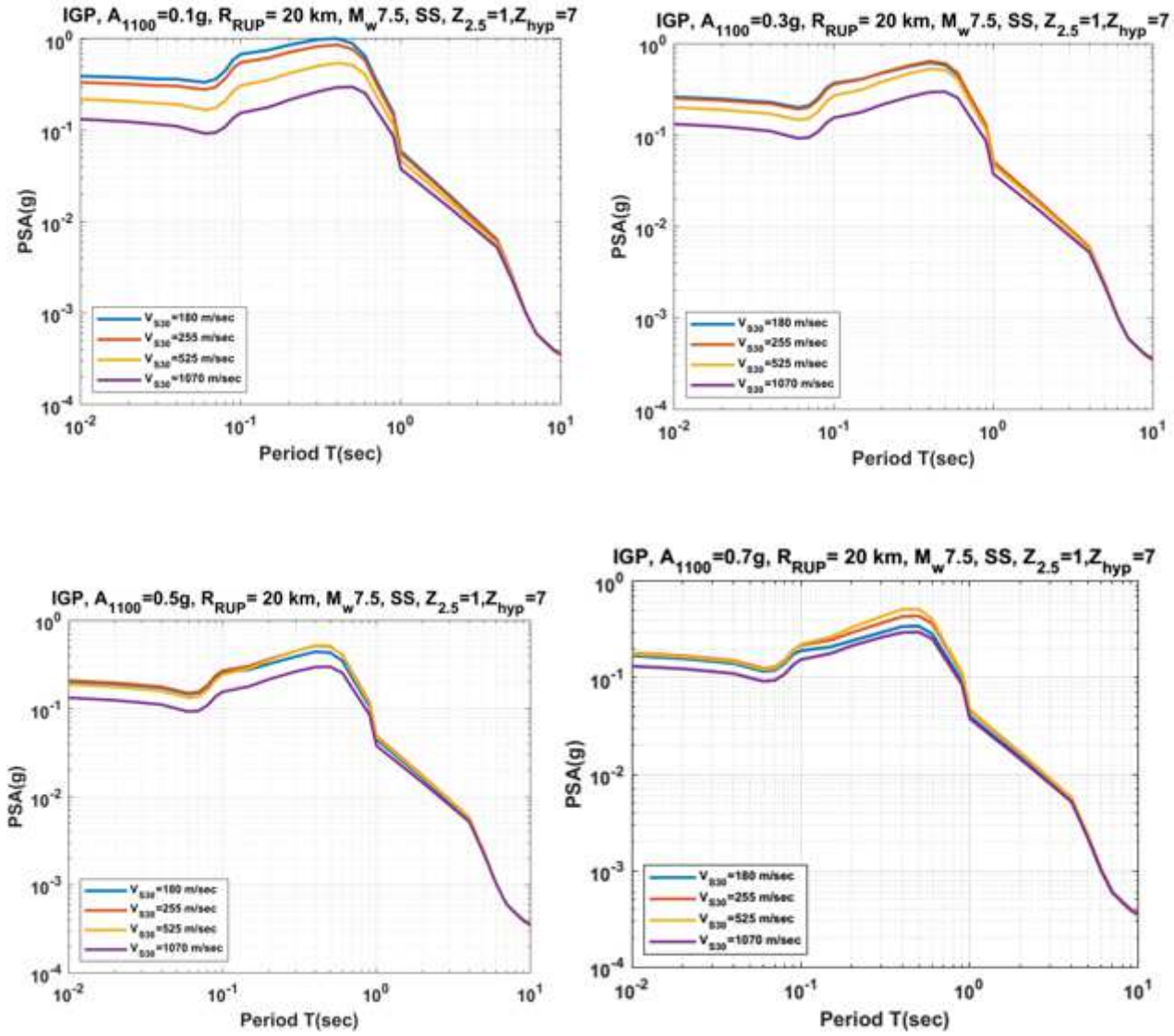

Figure 19

Scaling of PSA with site conditions and bedrock PGA for the IGP basin.

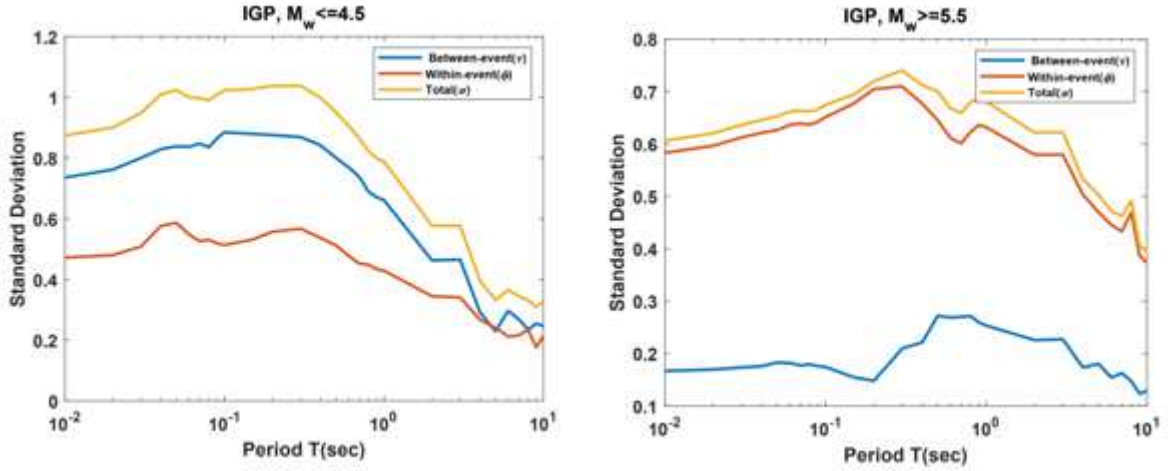

Figure 20

Aleatory standard deviations for the IGP model.

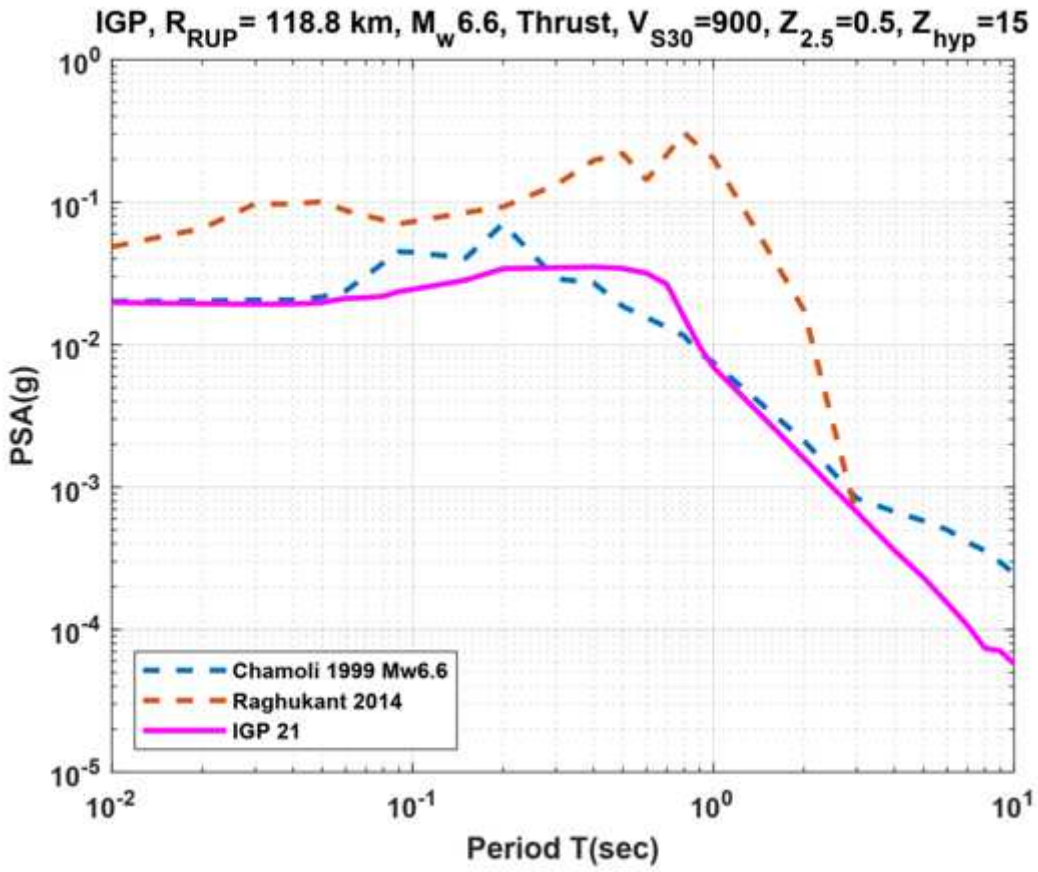

Figure 21

Shows spectral amplitude comparison of the developed equations for recorded site conditions VS30=900 m/sec using the recorded 1999 Chamoli earthquake 6.6 M.

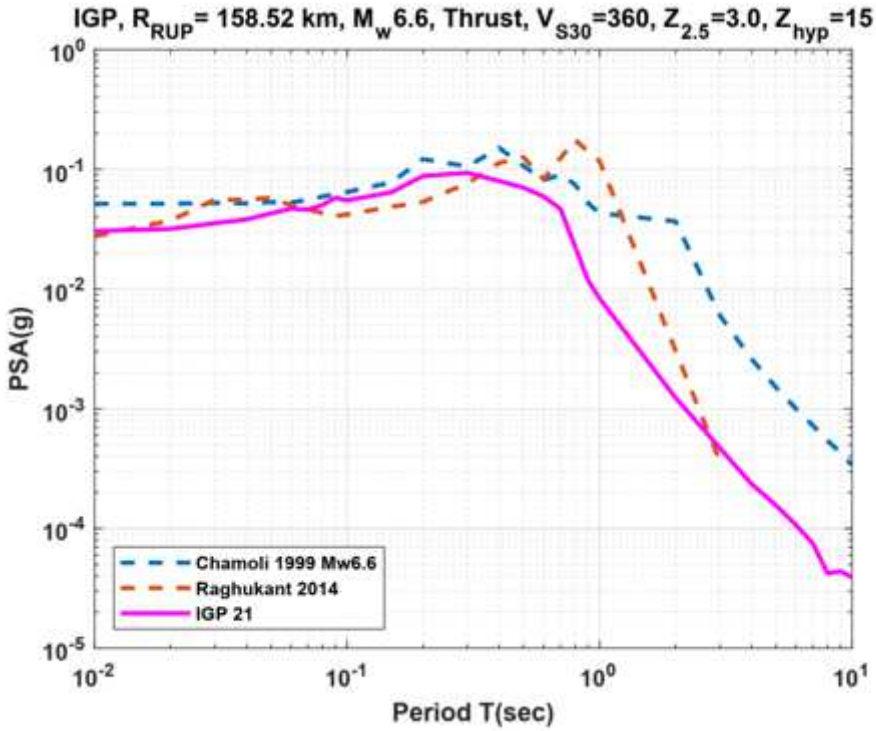

Figure 22

Shows spectral amplitude comparison of the developed equations for recorded site conditions VS30=360 m/sec using the recorded 1999 Chamoli earthquake 6.6 M.

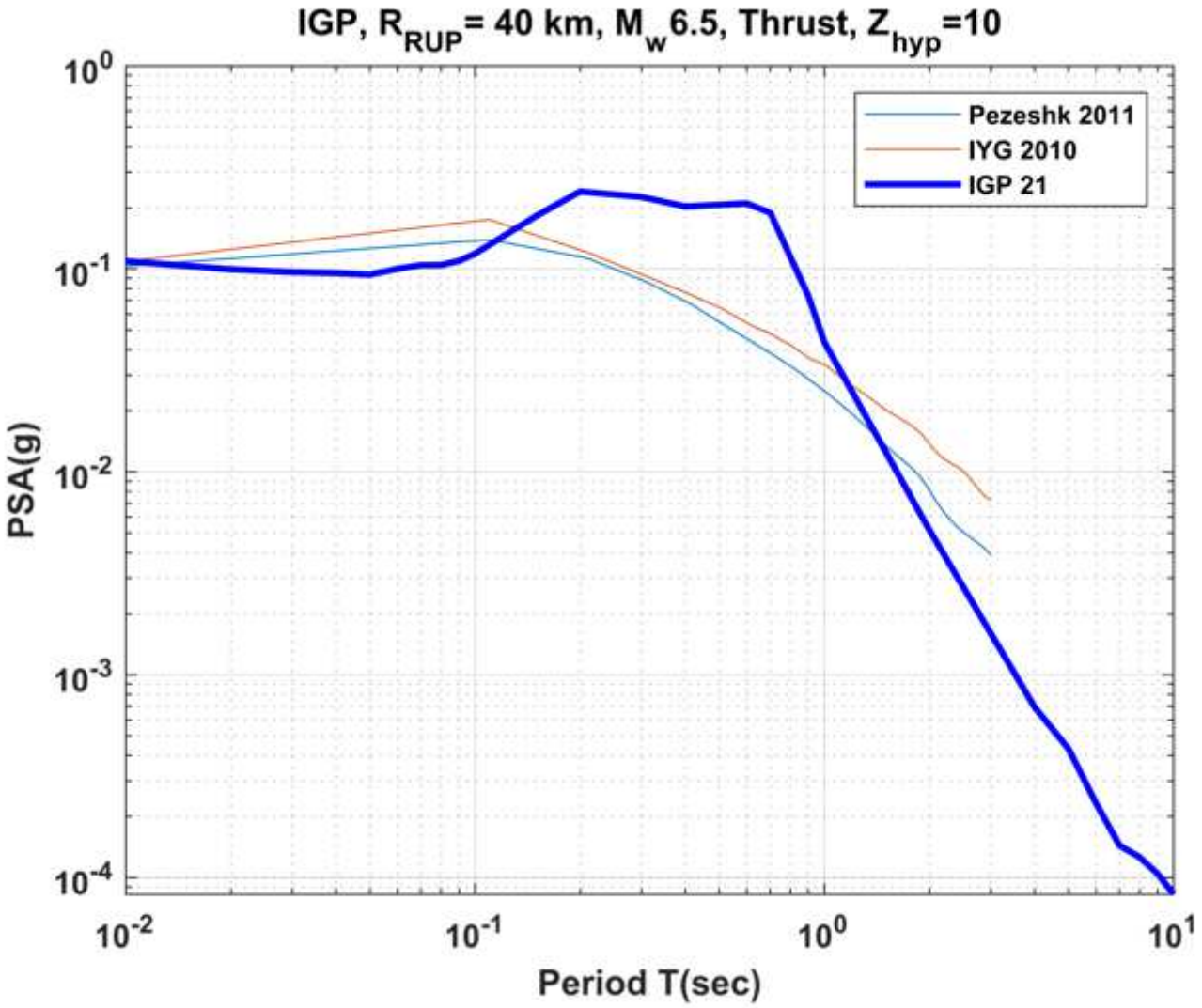

Figure 23

Shows spectral amplitude comparison of the developed different GMPEs for M6.5 at Rupture distance 40 Km.

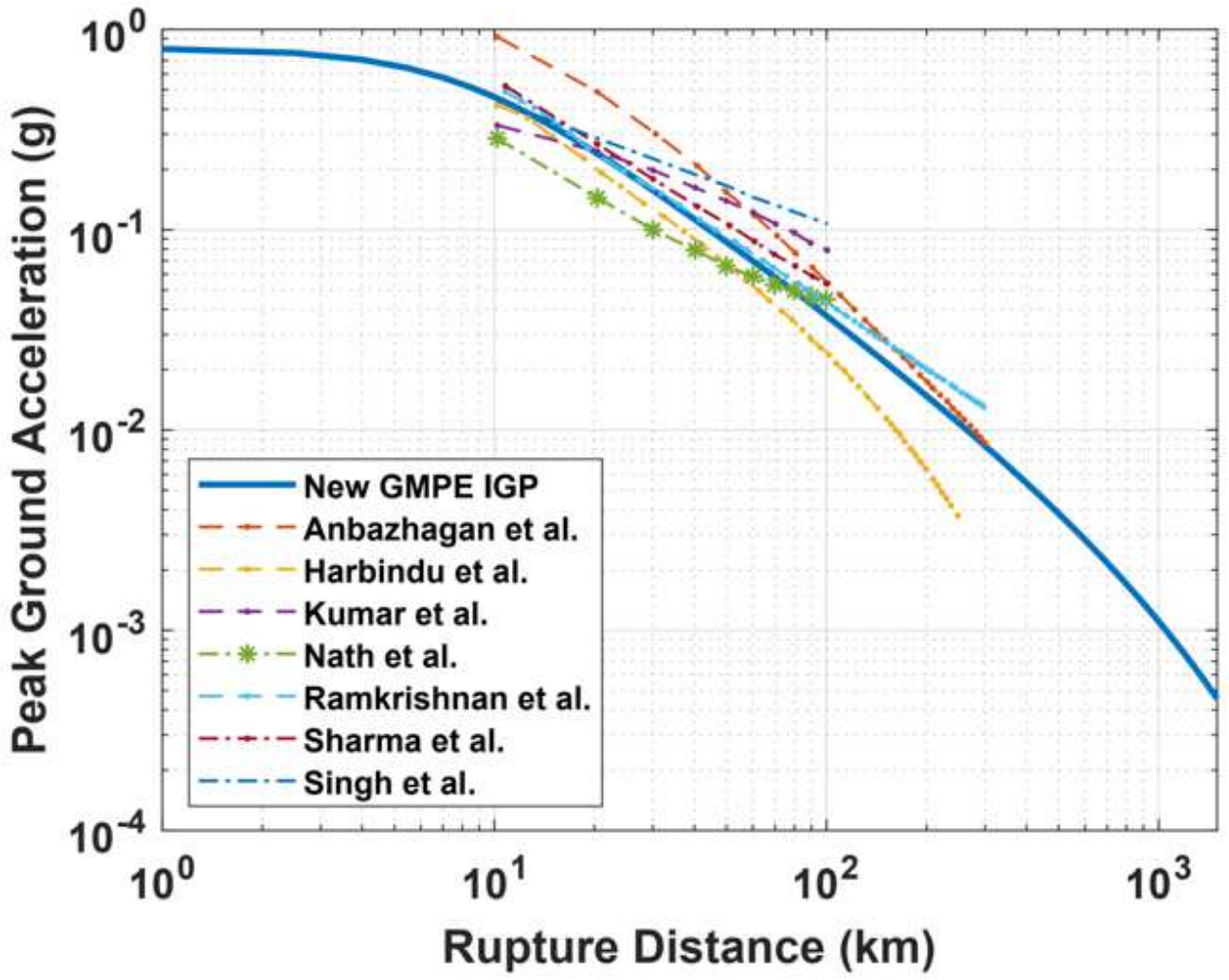

Figure 24

Shows comparison of the developed different GMPEs for M6.8 at different Rupture distances.